

German Aerospace Center
Institute of Propulsion Technology

IB 225 – 2012 A 06

Vincent Périer
Alexander Krumme

**Integration and Validation of S2-Flow
Computations for Aero-Thermodynamic
Pre-Design of Turbines**

Date: October 2012
Client: -
Applied for: Internship, ISAE-SUPAERO

Head of the Institute:
Prof. Dr.-Ing. R. Mönig

**Copying and communicating the contents of this document or any other information
– even of sections – to third parties only with permission of the client, of DLR-Gö**



Key words:

Pre design of turbines, automatic design chain, streamline curvature program, S2-flow computations, optimization tool *AutoOpti*, optimization criteria, validation of design data

Integration and Validation of S2-Flow Computations for Aero-Thermodynamic Pre-Design of Turbines**Abstract**

In order to speed up the design of turbomachines, the Turbine Department of the Institute is developing a turbine pre-design chain that should organize and accelerate all design steps prior to initial 3D-CFD calculations. Thus, DLR is developing generic tools for preliminary design projects of turbine design. This paper reports the activities led by DLR for turbine pre-design, focusing on advanced 2D-calculations and optimization.

The preliminary projects for the aero-thermodynamic design of turbines are supposed to provide reliable results in a short time. Nowadays the 3D-CFD is recognized for the precise results it can provide, but the significant computation times are yet a limitation for its use in preliminary projects. For the turbine pre-design, methods of fluid computation are chosen according to their computation rapidity more than the precision of the provided results. Hence 0-2D computation methods are used for the pre-design. The advantage of advanced 2D-computations for turbine pre-design is quickly introduced, before presenting the turbine pre-design chain developed by DLR. The main tools are then described separately.

The integration of S2-computations (i.e. SLC4T program code) in the turbine pre-design process should contribute to accelerate significantly the switch from one step to the next. With this work, some routines were implemented, so that 1D pre-design can be followed automatically by SLC4T computations for providing turbine map data files. Second big task for this work was to implement a preconfigured and general optimization process using *AutoOpti* for annulus geometry of turbines that could be quickly set up coming from *PrEDiCT* 1D pre-design. Many optimization criteria, such as the regions of interest of parameter values, are strongly problem-oriented. As regards S1-stream surfaces, human know-how is deeply involved when designing blade profiles. The complete automation of blade design itself is therefore not foreseen. However, it would be of interest to implement an automatic update of S2-flow computations input files, once the blades have been designed precisely. By this way the optimization process of the annulus contour could be performed on the turbine with updated blade parameters. Furthermore as HPT and LPT are optimized together, it could be of interest to optimize the inter turbine duct shape as well. The current optimization process as introduced with this work does not possess enough criteria, so as to provide a pertinent optimized size of the inter turbine ducts. Therefore in the future, SLC4T computations could be complemented by boundary layer computations in the inter turbine duct.

Table of contents

Introduction.....	1
1 Principle of turbine pre-design.....	1
1.1 Turbine pre-design chain.....	1
1.1.1 Introduction to 2D-computations for turbine pre-design.....	1
1.1.2 Overview of the turbine pre-design chain.....	2
1.2 Presentation of turbine pre-design tools.....	3
1.2.1 1D Pre-design.....	3
1.2.2 S2-flow computation.....	4
1.2.3 Turbine maps.....	5
1.2.4 Blade design.....	10
2 Implementation of S2-calculations.....	13
2.1 Streamline curvature throughflow theory.....	13
2.1.1 Quasi-normal stations.....	13
2.1.2 Formal equation of motion.....	14
2.1.3 Practical use of the equation of motion.....	14
2.2 Program Code SLC4T.....	16
2.2.1 Input quantities.....	16
2.2.2 1D-calculation of the airflow.....	17
2.2.3 2D-calculation of the meridional flow.....	18
3 Integration of the Program Code SLC4T.....	20
3.1 Task 1 - Calibration and validation of SLC4T-Calculations.....	20
3.1.1 SLC4T/3D-CFD Computation – Global flow properties.....	20
3.1.2 Calibration of the air cooling parameters.....	22
3.1.3 SLC4T/3D-CFD Computation – Local flow properties.....	25
3.2 Task 2 – Creation of turbine maps.....	26
3.2.1 First pre-design and turbine map.....	26
3.2.2 Implementation.....	28
3.2.3 Geometric design of Inter Turbine Ducts (ITD).....	29
3.2.4 Interpolation of the quasi-normal stations.....	32
3.2.5 Test case: TATT-5S-Turbine.....	33
3.3 Task 3 – Optimization of the annulus contour.....	36
3.3.1 2D-computations and optimization of the annulus contour.....	36
3.3.2 Tool AutoOpti.....	36

3.3.3	Implementation.....	37
3.3.4	Blade geometry updating.....	39
3.3.5	Optimization criteria.....	40
3.3.6	Test case: Hannover-Turbine.....	41
	Conclusion and prospects	46
	Acknowledgements	46
	References.....	47
	Appendix.....	48
	A1 - Conservation laws for the Streamline Curvature Method.....	48
	A2 – Outlet flow angle correlation	49

Introduction

The Institute of Propulsion Technology of the German Aerospace Center DLR focuses its research work on turbomachines used in power plants as well as in aircraft propulsion. In order to speed up the design of turbomachines, the Turbine Department of the Institute is developing a turbine pre-design chain that should organize and accelerate all design steps prior to initial 3D-CFD calculations. Thus, the DLR is developing generic tools for preliminary design projects of turbine design. This paper reports the activities lead by DLR for the turbine pre-design, focusing on advanced 2D-calculations and optimization.

1 Principle of turbine pre-design

The preliminary projects for the aero-thermodynamic design of turbines are supposed to provide reliable results in a short time. Nowadays the 3D-CFD is recognized for the precise results it can provide, but the significant computation times are yet a limitation for its use in preliminary projects. For the turbine pre-design, methods of fluid computation are chosen according to their computation rapidity more than the precision of the provided results. Hence 0-2D computation methods are used for the pre-design. The advantage of advanced 2D-computations for turbine pre-design is quickly introduced, before presenting the turbine pre-design chain developed by DLR. The main tools are then described separately.

1.1 Turbine pre-design chain

1.1.1 Introduction to 2D-computations for turbine pre-design

The 2D-computation methods for turbomachines have been developed in the early period of flow computation, before the emergence of 3D-CFD. Nowadays these 2D-codes are still appreciated for their quick computation times. According to the theory of Wu [1], these 2D-computations can be performed in two quasi-normal surfaces called S1 and S2 respectively. S1- and S2-computations provide complementary results as regards the flow properties over a blade rows cascade. An example of S1- S2-stream surfaces is shown in Figure 1.

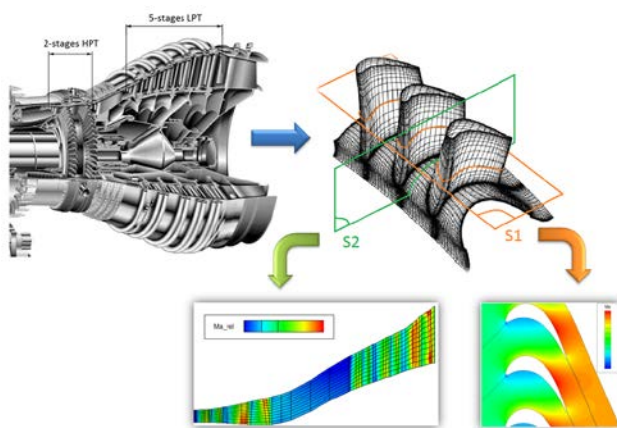


Figure 1: Overview of S1- S2-stream surfaces

- S1-stream surfaces are called blade-to-blade surfaces. The flow is computed in the circumferential and meridional direction, between two blade profiles, neglecting radial velocity components. Blade-to-blade computations are used to provide a distribution of the

flow properties between blade profiles. The massflow through a blade row can be calculated precisely by taking account of the smallest cross section, called the throat. The blade thickness distribution along the mean line of the profile is an important factor concerning the massflow. In most modern turbines indeed, the Mach number reaches $M_a = 1$ in the throat, which determines the flow velocity in the throat and consequently the massflow.

- S2-stream surfaces are called hub-to-tip surfaces. The flow is computed from the turbine inlet to the turbine outlet in meridional direction, averaging out all circumferential flow quantities. This would be equivalent to compute the flow on a mean surface. S2-computations provide a radial distribution of the flow properties in the turbine annulus.

1.1.2 Overview of the turbine pre-design chain

As seen previously, S1- and S2-computations are useful tools for turbine pre-design. These computations are used in several steps of the turbine pre-design process. In order to link them, 1D pre-design calculation methods and procedural ways have been developed by DLR. The integration of S2-flow computations in the pre-design process has been the purpose of the internship. An overview of the turbine pre-design chain is shown Figure 2.

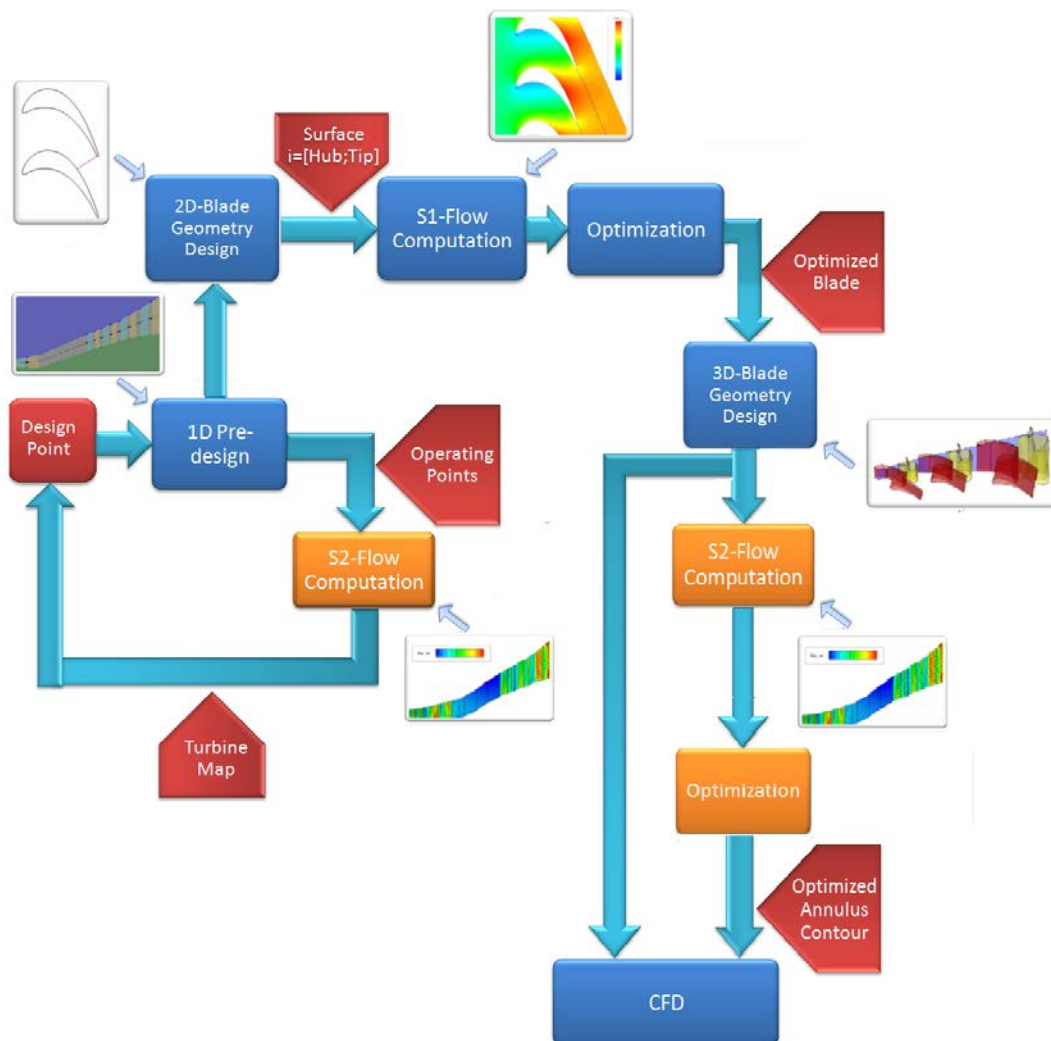


Figure 2: Turbine pre-design chain

According to the aero-thermodynamic conditions imposed in the turbine inlet and outlet, and according to the expected mechanical power to be provided by the turbine, a *Design Point* is chosen. A first *1D Pre-design* can be performed with analytical correlations and loss models, in order to estimate the aero-thermodynamic flow parameters and states. At this step, the number of stages can be determined, a first annulus contour geometry can be designed, and the first blade geometrical parameters can be estimated. This *1D Pre-design* is followed by *S2-Flow Computations* at several *Operating Points*, so as to generate *Turbine Maps*, which provide an overview of the turbine behavior. Thus, the *Design Point* can be adjusted if needed. At this step, the *1D Pre-design* provides enough geometrical parameters to perform a 3D geometrical design of the blade rows. Some S1-flow surfaces are chosen, and the *S1-Flow Computations* are performed on the blade profiles. Eventually, the geometrical design is improved according to the *S1-Flow Computations* results. The blade profile shapes are then altered in an *Optimization* process according to aero-thermodynamic criteria. The optimized blade profiles are then combined so as to provide 3D blade geometry that can be used for the next flow computations. This step is followed by *S2-Flow Computations* that provide fields of aero-thermodynamic flow properties over the turbine annulus. An *Optimization* process is then performed on the annulus contour geometry. The optimized annulus together with 3D-oriented optimized blade profiles, form a solid data base for 3D-CFD input.

1.2 Presentation of turbine pre-design tools

1.2.1 1D Pre-design

A 1D Pre-design can be performed with the definition of the design point. In most applications the design point is determined by the turbine’s external environment, which defines the shaft power to be provided and the rotational speeds of the spools. When the turbine is to be used in aircraft engines, the power to be provided and the spools’ rotational speeds are determined by the high/low pressure compressor. The turbine aero-thermodynamic and geometrical inlet conditions are useful to perform the 1D Pre-design. These parameters are listed Figure 3.

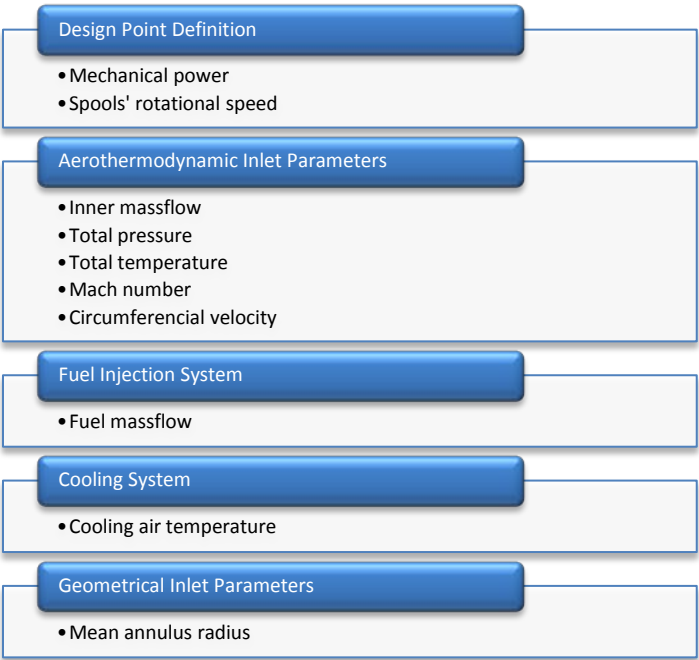


Figure 3: 1D Pre-design Input parameters

Furthermore, some analytical models are used to design the blade-rows. They are summed up in Figure 4.

Leading Edge/Trailing Edge Angles Calculation	Pitch Calculation	Flow Outlet Deviation
Velocity Triangles	Zweifel Model	Sjolander Model

Figure 4: Blade design models

- Leading Edge/Trailing Edge Angles Calculation:** the usual Velocity Triangle Method is used according to the Chasles Relation: $\vec{V}_{flow/0} = \vec{W}_{flow/rot} + \vec{U}_{rot/0}$. This method provides the inlet and outlet flow angle for each blade row of a cascade, according to the variations of total enthalpy over each rotor, which are defined so as to deliver the expected shaft power. The leading edge and trailing edge angles can thus be calculated for each blade row.
- Pitch Calculation:** the work of Zweifel is used to define an optimum pitch/chord ratio. Zweifel suggested a correlation (1.1) giving the lift coefficient C_y of a blade row as function of the pitch/chord ratio $\frac{t}{l_x}$ and the upstream and downstream flow angles, α_{in} and α_{out} respectively:

$$C_y = 2 * \frac{t}{l_x} * (tan\alpha_{out} + tan\alpha_{in}) * cos^2\alpha_{out} \quad (1.1)$$

The optimum pitch/chord ratio is reached as the lift coefficient is close to 0.8.

- Deviation:** The pressure difference between the pressure side and the suction side generates a flow deviation downstream of the trailing edge, which means that the streamline is no more tangential to the trailing edge. This flow deviation is quantified with the help of the stagger angle. A correlation presented by Sjolander in [3], is used to estimate this stagger angle. Generally the outlet flow angle is a little lower than the trailing edge angle, because the pressure is higher on the pressure side than on the suction side.

1.2.2 S2-flow computation

The 1D pre-design can be completed by a S2-flow computation, in order to provide a radial distribution of the flow properties in the turbine annulus. Since S2-flow computations are in the very heart of the subject, they are presented in detail in paragraph 2. A short example only is presented as illustration. S2-flow computations have been performed on the TPS-Turbine, a 3 stages high pressure turbine that will be used on a test bench for fans and compressors. The compressor requiring the higher power imposes the design point. The axial velocity is plotted Figure 5.

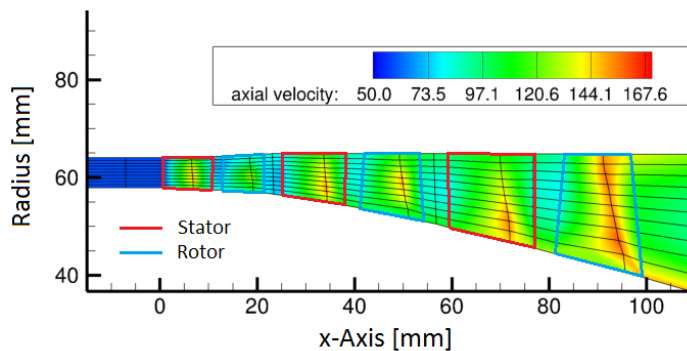


Figure 5: TPS-Turbine - Axial velocity

In most cases turbine annuli are designed in a way that axial velocity V_x is kept constant. The fluid expansion over the turbine induces a decrease of the flow density ρ . Since the massflow $\dot{m} = A\rho V_x$ is conserved through the turbine duct, the axial velocity V_x is kept constant thanks to the slight divergent duct. Thus, upstream and downstream of a blade row, the axial velocity is more or less constant. Over a blade row, the fluid is accelerated. The cross section A indeed is the lowest in the throat. The axial velocity V_x therefore increases in the throat.

The circumferential velocity is plotted Figure 6. The flow is especially deviated downstream of the stators, so that the relative flow velocity is tangential to the rotor inlet. The flow deviations over the rotor induce an energy transfer between the fluid and the rotor, which provides a mechanical power to the spool.

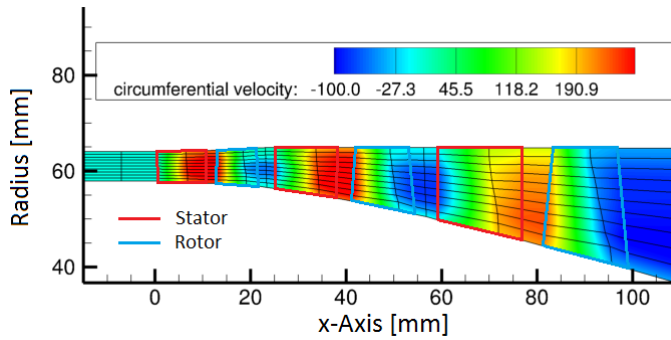


Figure 6: TPS-Turbine - Circumferential velocity

1.2.3 Turbine maps

Turbine maps are providing an overview of the whole behavior of the turbine, which is really helpful at the beginning of the design process. A turbine map has to be calculated for each spool of the turbine. The pressure ratio commonly used for compressor maps is in most cases replaced by the specific work. The main purpose of a turbine indeed is to provide energy to a spool. The rotational speed or the massflow are plotted on the x-axis of turbine maps. Thanks to the use of the corrected massflow, the turbine map is independent from the total temperature and total pressure. The massflow indeed is given by (1.2).

$$\dot{m} = A\rho M_x \frac{p_t}{\sqrt{T_t}} \left(1 + \frac{\gamma-1}{2} M^2\right)^{\frac{\gamma-1}{2(\gamma-1)}} \sqrt{\frac{\gamma}{R}} \quad (1.2)$$

\dot{m} : massflow,
 A : annulus cross section,
 ρ : fluid density,
 M_x : axial Mach number,
 p_t : total pressure,
 T_t : total temperature,
 $\gamma = \frac{c_p}{c_v}$ specific heat capacity ratio,
 M : Mach number,
 R : specific gaz constant.

Hence, if the turbine map is set with the help of the corrected massflow $\dot{m}_{corr} = \dot{m} \sqrt{\frac{T_t p_o}{T_o p_t}}$, where p_o and T_o are reference values, the turbine map is valid independently of the pressure and

temperature conditions. A turbine map of the TPS-Turbine is given Figure 7. On the x-axis, the quantity $N * \dot{m}$ is plotted, where N is the spool rotational speed.

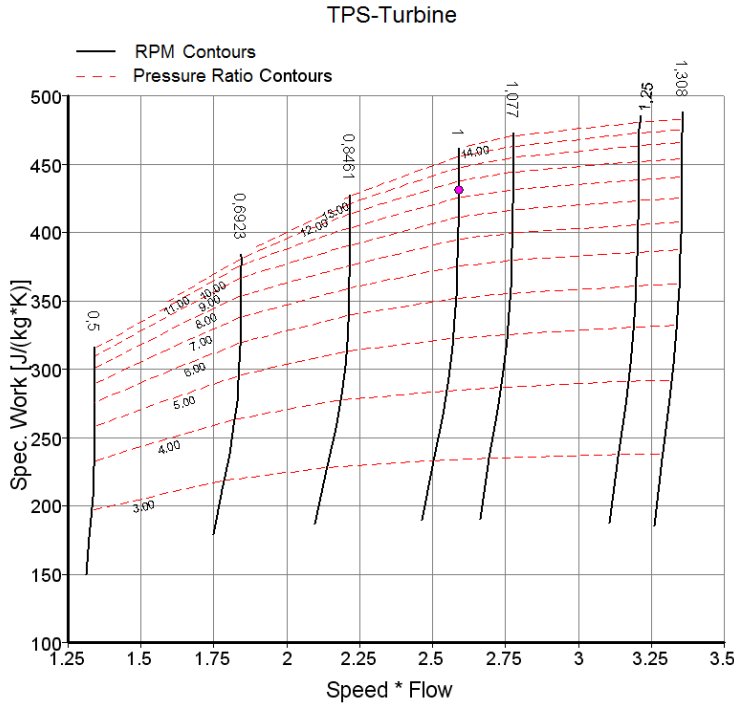


Figure 7: TPS-Turbine Map – SpecificWork(Speed*Flow), Speed, PressureRatio

The specific work delivered by the flow to the turbine can be deduced from the pressure ratio $PR = \frac{pt_{in}}{pt_{out}}$ thanks to an isentropic relation, which relates the total temperature loss and the total pressure loss:

$$\left(\frac{pt_{in}}{pt_{out}}\right)^{\frac{\gamma-1}{\gamma}} = \frac{Tt_{in}}{Tt_{outis}} \quad (1.3)$$

The total enthalpy ΔH extracted from the flow to the turbine results of the total temperature difference between the turbine inlet and outlet. The total enthalpy ΔH and the isentropic enthalpy ΔH_{is} are given by :

$$\Delta H = C_p \cdot (T_{t_{in}} - T_{t_{out}}), \quad (1.4)$$

$$\Delta H_{is} = C_p \cdot (T_{t_{in}} - T_{t_{outis}}). \quad (1.5)$$

Thanks to the isentropic efficiency $\eta_{is} = \frac{\Delta H}{\Delta H_{is}}$, the total enthalpy can be written :

$$\Delta H = \eta_{is} \cdot C_p \cdot T_{t_{in}} \cdot \left[1 - (PR)^{\frac{\gamma-1}{\gamma}}\right]. \quad (1.6)$$

Thus the specific work $SW = \frac{\Delta H}{T_{t_{in}}}$ can be written:

$$SW = \eta_{is} \cdot C_p \cdot \left[1 - (PR)^{\frac{\gamma-1}{\gamma}}\right]. \quad (1.7)$$

The more energy extracted from the flow, the higher is the pressure ratio PR . Therefore the specific work SW increases with the pressure ratio PR . The influence of the isentropic efficiency can be seen Figure 8.

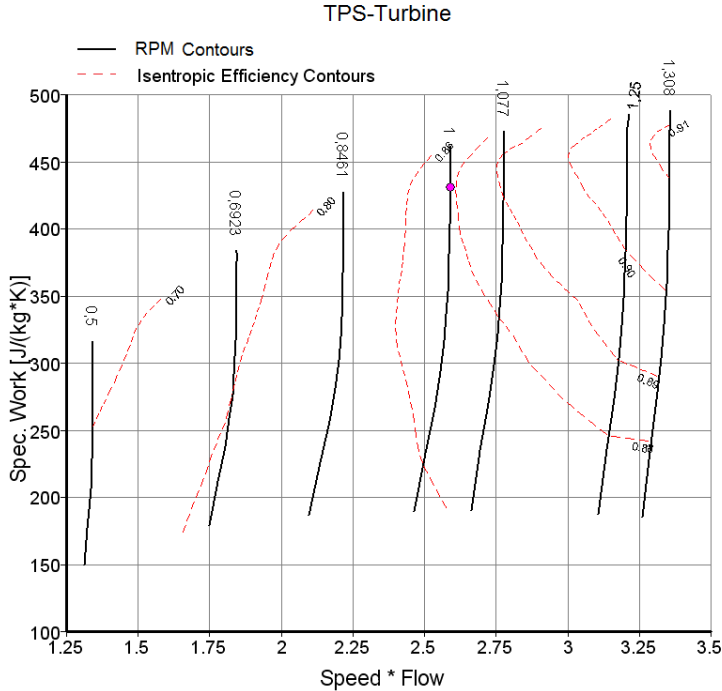


Figure 8: TPS-Turbine Map - SpecificWork(Speed*Flow), Speed, Efficiency

The general trend of the isentropic efficiency is to increase when $N * \dot{m}$ increases. The low isentropic efficiency that is to be seen for low $N * \dot{m}$ induces a decrease of the specific work, according to equation (1.7), which can be seen on Figure 7.

Turbine maps are helpful for the following applications:

- Overview of the whole turbine:** in most cases, a turbine designed for aircraft engines consists in a high pressure turbine (HPT) and a low pressure turbine (LPT) powering a HP-shaft and a LP-shaft respectively. The combination of the turbine maps of each shaft is really helpful to provide the global characteristics of the turbine. The pressure ratio of a 2-shaft turbine $\frac{pt_{in}}{pt_{out}}$ indeed is given by: $\frac{pt_{in}}{pt_{out}} = \frac{pt_{in_1}}{pt_{out_1}} * \frac{pt_{in_2}}{pt_{out_2}}$, where $\frac{pt_{in_1}}{pt_{out_1}}$ and $\frac{pt_{in_2}}{pt_{out_2}}$ are depicted on the turbine maps of shaft 1 and shaft 2. According to the continuity equation, the massflow is conserved over the turbine annulus. The massflow, the HPT- and LPT-pressure ratios as well as the shaft's rotational speeds are then combined. Whether a turbine is adapted for a given operating point can be easily checked on turbine maps.
- Overview of the power transmission in the turbomachine:** a turbine designed for a turbomachine is usually supposed to provide mechanical power to a compressor. In this case, turbine maps and compressor maps can be matched in order to ensure the common operation of the compressor with the turbine. As illustration, a turbine map of the TPS-Turbine is provided Figure 9. The TPS-Turbine indeed is supposed to provide mechanical power for a compressor test bench. Therefore it is of great interest to determine the power

that can be provided as function of the rotational speed. The computations have been performed with $\frac{pt_{in}}{ps_{out}} = 12.8$, and $T_{t_{in}} = 330K$. It is interesting to note that according to equation (1.2), the massflow depends only on the total inlet temperature and total inlet pressure, as the pressure ratio $\frac{pt_{in}}{ps_{out}}$ is fixed. The power is all the higher, than the flow energy decreases by passing through the turbine. Therefore the power is all the higher than the outlet total pressure is low. The design point is determined by a compressor that needs $357kW$ and whose rotational speed is $26000 RPM$. These conditions can be realized if the test bench provides a turbine inlet total pressure $pt_{in} = 18 bar$.

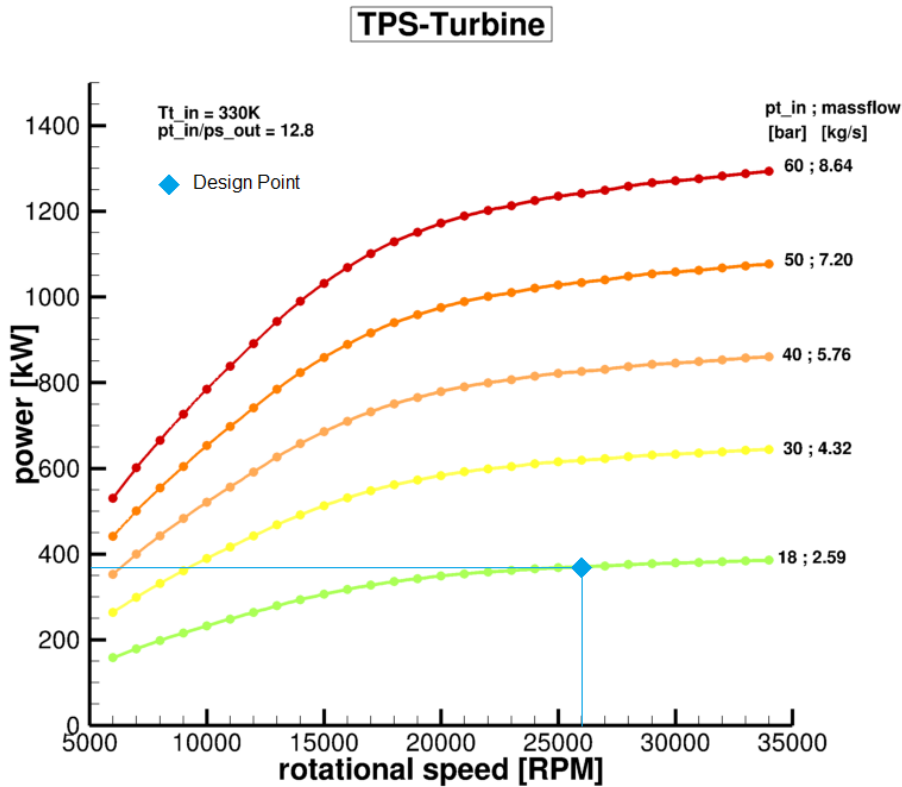


Figure 9: TPS-Turbine Map - Power(Speed)

The performance of a turbine is in a large part linked to the massflow passing through it. The adjustment and setting of the massflow are therefore of interest. On the turbine map plotted Figure 10, the massflow is depicted as function of the total pressure ratio for several relative speeds $N_{rel} = \frac{N}{N_{des}}$, where N is the spool rotational speed, and $N_{des} = 26000 RPM$ the design rotational speed. On Figure 10, the relation between the rotational speed and the massflow is clearly noticeable. As the expansion ratio is low, the high outlet pressure limits the flow velocity. Therefore the massflow is low for low pressure ratios. As the expansion ratio increases, the flow is accelerated. As the Mach number reaches $M_a = 1$ in the throat, the corrected massflow has reached its maximal value. Even if the expansion ratio increases further, the corrected massflow is limited to its maximal value. The expansion ratio and the rotational speed have an influence on the energy extracted from the fluid to the spool. Thus, for a given pressure ratio, the more energy is extracted from the flow, the higher is the rotational speed. The flow kinetic energy and consequently the massflow trend to decrease, when the rotational speed increases.

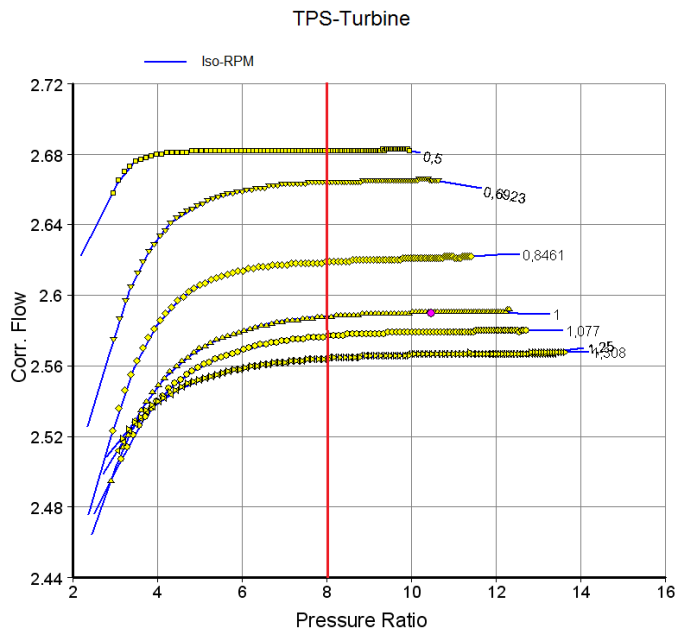


Figure 10: TPS-Turbine Map. Corr.Flow-Pressure Ratio

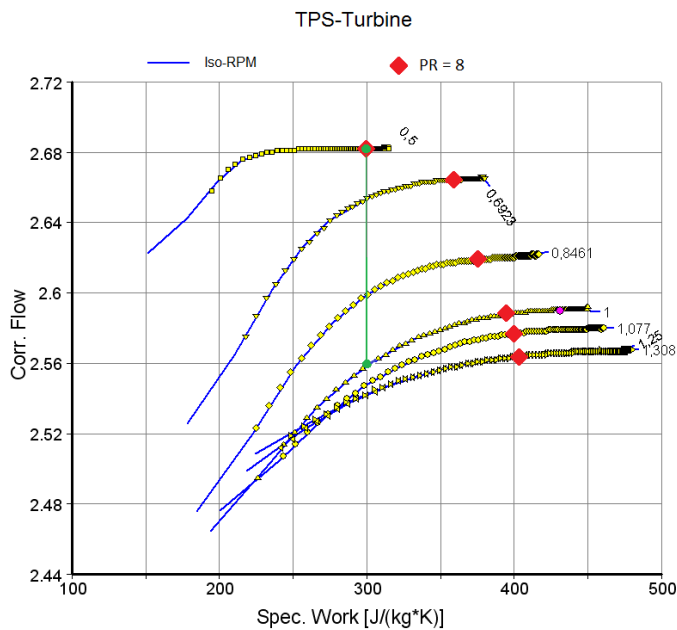


Figure 11: TPS-Turbine Map - CorrectedFlow(SpecificWork), Speed

The pressure ratio and the specific work are related by the efficiency. Figure 11 shows the operating points for which $PR = 8$. As the rotational speed increases, the specific work is higher, although the pressure ratio is set to $PR = 8$. The efficiency indeed increases along the iso-line $PR = 8$, as the rotational speed increases. The influence of the pressure ratio PR and the rotational speed N on the turbine efficiency can be explained thanks to an analysis of the interaction between the flow and the blades. According to the pressure ratio and the spool rotational speed, the blade geometry is more or less adapted to the actual flow, which has an influence on the efficiency. Therefore a review of the blade design principle will help to understand the influence of the pressure ratio and rotational speed on the efficiency.

1.2.4 Blade design

During the 1D pre-design, the first parameters of the blades are chosen, according to the design point. Some parameters can be adjusted thanks to the information provided by the turbine map. Then the blades are designed precisely: at first the profiles are designed for several S1-surfaces, what leads to a 3D assembly. An overview of the blade rows of the TPS-Turbine is given Figure 12.

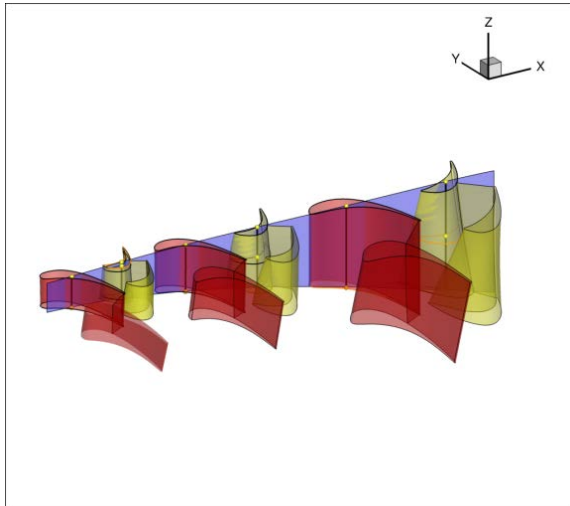


Figure 12: TPS-Turbine - 3D-blade design

The blades profiles are designed according to the Velocity Triangle Method. A review of this method is given, in order to explain the influence of the pressure ratio and the rotational speed on the efficiency, as it can be observed on the TPS-Turbine map (Figure 8). Figure 13 illustrates a typical application of the Velocity Triangle Method.

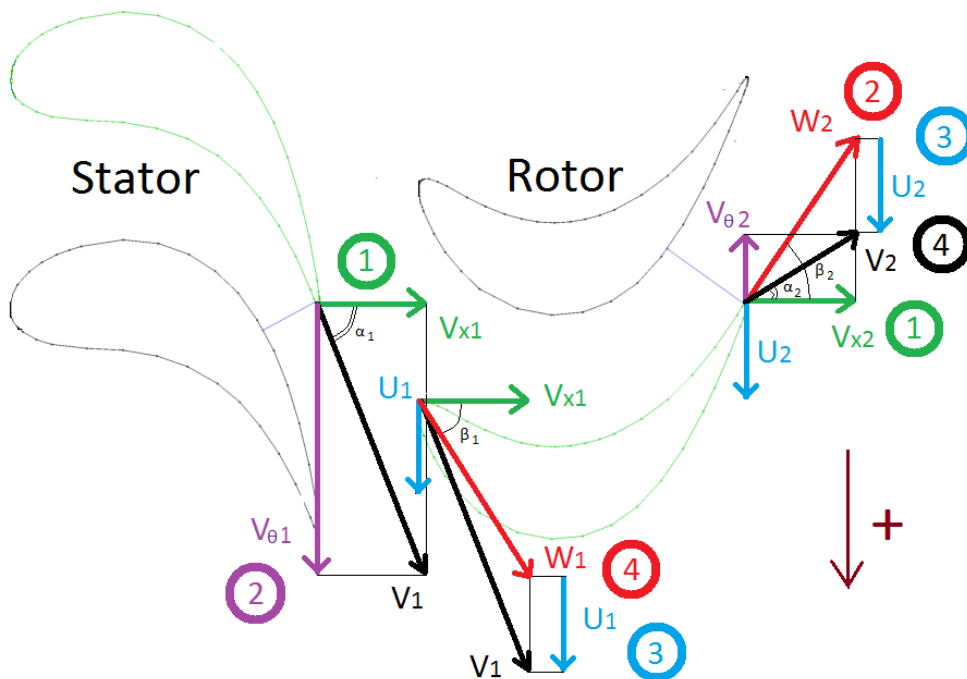


Figure 13: Velocity Triangle Method

1. The massflow \dot{m} is determined to a large extent by the axial velocity V_x , as it can be seen by writing the definition of the massflow: $\dot{m} = \rho A V_x$. According to the massflow conservation, the flow is accelerated through the throat, but in most cases the turbine annulus is designed so that the axial velocity V_x is constant over the turbine in non-bladed areas. The axial velocity V_x can therefore be considered identical in the trailing edge and in the leading edge of a blade row. Thus we have: $V_x = V_{x1} = V_{x2}$.
2. As explained in paragraph 1.2.1, the stator outlet flow angle is determined by the stator trailing edge angle. At first approximation, the direction of the velocity V_1 in the stator trailing edge can be determined: $\tan \alpha_1 = \frac{V_{\theta 1}}{V_{x1}}$. Likewise, the direction of the relative velocity W_2 along the rotor trailing edge is given by: $\tan \beta_2 = \frac{W_{\theta 2}}{V_{x2}}$.
3. The spool rotational speed $U_2 = r_2 \omega$, is controlled by the input parameters. In aircraft engines, it can be controlled with the fuel injection. According to the relation $V_{\theta 2} = W_{\theta 2} + U_2$, the circumferential velocity $V_{\theta 2}$ can be determined. Hence the absolute flow angle α_2 can be determined in the rotor trailing edge by: $\tan \alpha_2 = \frac{V_{\theta 2}}{V_{x2}}$.
4. The pressure ratio over the stage row induces a variation of total enthalpy ΔH in the rotor. According to the Euler-Equation $\Delta H = \Delta(U \cdot V_{\theta})$, the total enthalpy variation over the rotor induces the flow deviation. In the case of a cylindrical streamtube, we have: $U = U_1 = U_2$. Hence the Euler-Equation reads: $\Delta H = U \cdot (V_{\theta 2} - V_{\theta 1})$. Thus the enthalpy variation imposed by the pressure ratio is related to the flow deviation: $\Delta H = U \cdot V_x \cdot (\tan \alpha_2 - \tan \alpha_1)$. Since the massflow \dot{m} is proportional to the axial velocity V_x , it is common to plot the specific work ΔH as function of the quantity $\dot{m} \cdot \omega$. These turbine maps depict therefore the flow deviation.

These considerations are helpful to explain the efficiency variations on turbine maps. The efficiency is raised if:

- the direction β_1 of the relative velocity W_1 is adapted to the rotor leading edge angle,
- the direction α_2 of the absolute velocity V_2 is adapted to the leading edge angle of the next stator.

If the operating point is modified, the angles β_1 and α_2 may be modified, which have an influence on the efficiency. However the directions β_1 and α_2 can be kept constant if the axial velocity V_x and the rotational speed U are varying proportionally. The flow rate $\varphi = \frac{V_x}{U}$ is useful to quantify the change of the axial velocity V_x with the rotational speed U . If the flow rate φ is constant, the flow deviations β_1 and α_2 are not modified, as Figure 14 shows. Tanks to the load factor $\psi = \frac{\Delta H}{U^2}$, the Euler-Equation can be written: $\psi = \varphi \cdot (\tan \alpha_2 - \tan \alpha_1)$. The absolute rotor inlet angle α_1 is defined by the stator outlet geometry. If the load factor φ is offset from its optimal value, the flow deviations β_1 and α_2 are modified, and the load factor ψ is modified.

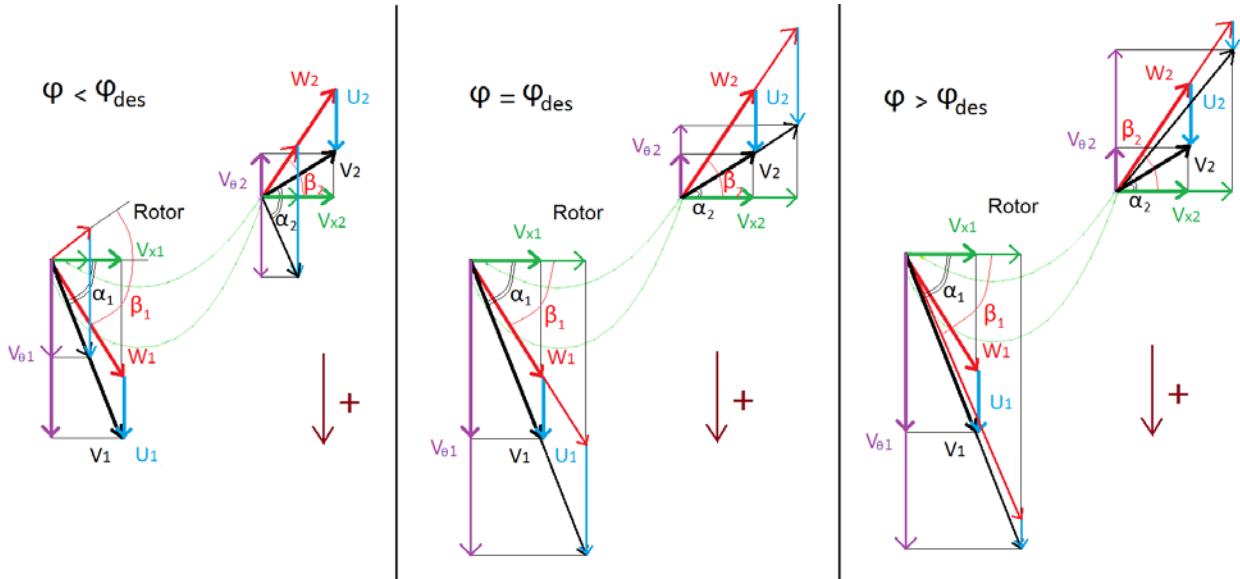


Figure 14: Influence of the Flow Rate on the Load Factor

The blade profiles are designed for the design point, so as to provide a satisfying efficiency. The design point determines the design flow rate $\varphi_{des} = \frac{V_x}{U_{des}}$. As soon as the flow rate is modified, the axial velocity V_x and the rotational speed U are no more varying proportionally, which has an influence on the efficiency. This criterion is used to explain the efficiency variations on the turbine map plotted on Figure 8. We assume that the turbine is operating to its design point.

If $N \cdot \dot{m}_{corr} = const.$, any decrease of the specific work ΔH implies a decrease of the flow deviation, according to the Euler-equation $\Delta H = U \cdot V_x \cdot (\tan \alpha_2 - \tan \alpha_1)$. The absolute rotor inlet flow angle α_1 is given by the stator outlet geometry. Therefore α_2 is going to be modified. According to the iso-RPM depicted on Figure 8, the rotational speed U slightly increases, what means that the massflow \dot{m} and consequently the axial velocity V_x slightly decrease. Therefore the flow rate $\varphi = \frac{V_x}{U}$ decreases, and $\varphi < \varphi_{des}$. Thus the absolute rotor outlet flow angle α_2 is no more adapted to the next stator leading edge, as Figure 14 shows. As regards the rotor inlet, the absolute velocity V_1 , tangential to the stator trailing edge, decreases and therefore $V_{\theta 1}$ decreases as well. Since U increases, the relative rotor inlet velocity $W_{\theta 1} = V_{\theta 1} - U$ decreases. The relative rotor inlet flow angle β_1 is therefore no more adapted to the blade profile. As a result, the efficiency decreases.

If $\Delta H = const.$, any decrease of $N \cdot \dot{m}_{corr}$ implies a decrease of $U \cdot V_x$. Thanks to Figure 11, it can be seen that, for a given specific work ΔH , a significant decrease of the rotational speed U implied a slight increase of the corrected massflow \dot{m}_{corr} . For instance, for $\Delta H = 300 J.kg^{-1}.K^{-1}$, the corrected massflow \dot{m}_{corr} increases from 2.56 to 2.58, when the rotational speed N_{rel} decreases from 1 to 0.5. Thus, the corrected massflow \dot{m}_{corr} and the rotational speed N_{rel} are not varying proportionally. The axial velocity V_x increases, whereas the rotational velocity U decreases. Therefore the flow rate $\varphi = \frac{V_x}{U}$ increases and $\varphi > \varphi_{des}$. This induces a deviation of the relative rotor inlet flow angle β_1 . The slight increase of the axial velocity V_x induces an increase of the circumferential velocity $V_{\theta 1}$, whereas the rotational speed U decreases significantly. Consequently the relative circumferential velocity $W_{\theta 1} = V_{\theta 1} - U$ deeply increases. Thus, the relative flow angle $\beta_1 = \arctan\left(\frac{W_{\theta 1}}{V_x}\right)$ increases. Hence, the flow angle β_1 is no more adapted to the rotor inlet geometry. As

regards the rotor outlet, the outlet angle α_2 is modified, because the rotational speed U decreases. Therefore the flow is no more adapted to the next stator inlet, what induces a decrease of the efficiency.

Beyond these considerations of theoretical aerodynamics, it is to know that the efficiency depends on the load factor $\psi = \frac{\Delta H}{U^2}$. The efficiency increases when the load factor ψ decreases. Theoretically, it would be of interest to design low loaded rows, with low flow deviations. However that would lead to several row stages, and would consequently increase the engine weight. That is the reason why turbines designed for aircraft engines are high loaded.

2 Implementation of S2-calculations

Two S2-calculations have evolved for the design of turbomachinery: the streamline curvature and the matrix throughflow. These methods provide both satisfying results for subsonic flows. However, the supersonic flows are easily calculated by using the streamline curvature. Since the flow through the blade row outlets is transonic in most of the modern turbines, a 2D-code using the streamline curvature has been implemented for the turbine pre-design.

2.1 Streamline curvature throughflow theory

S2-calculations implemented by the DLR are based on the streamline curvature throughflow theory. This theory and its application are quickly presented.

2.1.1 Quasi-normal stations

2D-calculations using the streamline curvature theory are performed on a mean stream surface. The flow quantities are actually mean values in circumferential direction. The flow quantities are calculated along a number of lines on this 2D-mean surface, that are called quasi-normal stations, because the streamlines are supposed to be roughly perpendicular to these stations. An overview of a typical streamline curvature grid is plotted Figure 15.

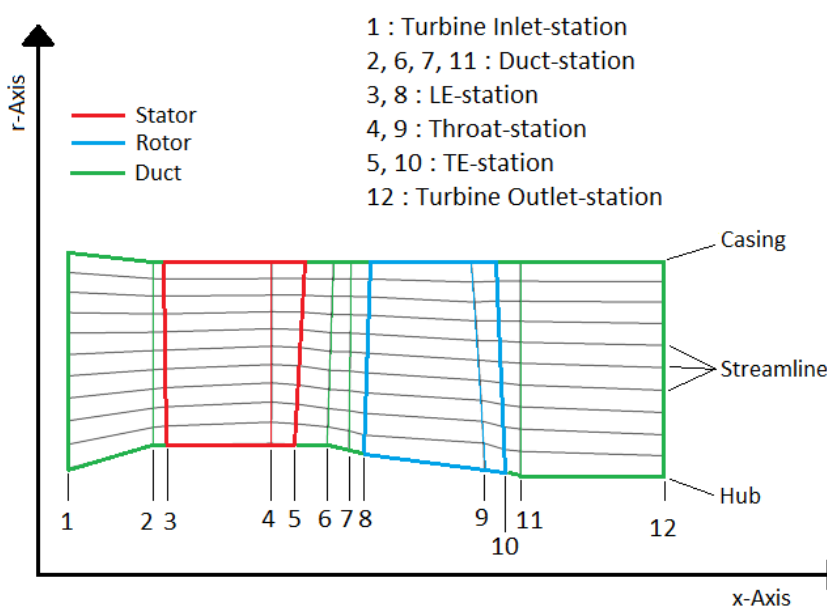


Figure 15: Quasi-normal stations (Fox-Turbine)

The flow quantities are calculated in the nodes by crossing of quasi-normal stations and meridional streamlines. The duct-stations are pure lines, whereas the leading edge stations, throat stations and trailing edge stations can match the blade shape. The method used here is a throughflow method, because some stations, the throat-stations indeed, are set between the leading edge and the trailing edge of the blades. These stations are particularly interesting, because they determine the massflow, and hence the outlet flow angle.

2.1.2 Formal equation of motion

The equation of motion used for the streamline curvature method, is written in a cylindrical polar system (x, r, θ) , which is rotating with a blade row at constant angular velocity ω . For inviscid, steady flow, the equation of motion is:

$$(\bar{W} \cdot \bar{\nabla}) \cdot \bar{W} = -\frac{1}{\rho} \bar{\nabla} p + \omega^2 \bar{r} - 2\bar{\omega} \wedge \bar{W} \quad (2.1)$$

\bar{W} is the relative flow velocity, $\omega^2 \bar{r}$ the inertial force, and $2\bar{\omega} \wedge \bar{W}$ the Coriolis force exerted by the row on the flow. In the cylindrical polar system (x, r, θ) , we can write:

$$W_r \frac{\partial W_x}{\partial r} + W_x \frac{\partial W_x}{\partial x} + \frac{W_\theta}{r} \frac{\partial W_x}{\partial \theta} = -\frac{1}{\rho} \frac{\partial p}{\partial x} \quad (2.2)$$

$$W_r \frac{\partial W_r}{\partial r} + W_z \frac{\partial W_r}{\partial z} - \frac{W_\theta^2}{r} + \frac{W_\theta}{r} \frac{\partial W_r}{\partial \theta} - 2\omega W_\theta - \omega^2 r = -\frac{1}{\rho} \frac{\partial p}{\partial r} \quad (2.3)$$

$$W_r \frac{\partial W_\theta}{\partial r} + W_z \frac{\partial W_\theta}{\partial z} + \frac{W_\theta W_r}{r} + \frac{W_\theta}{r} \frac{\partial W_\theta}{\partial \theta} + 2\omega W_r = -\frac{1}{\rho r} \frac{\partial p}{\partial \theta} \quad (2.4)$$

The flow is supposed axisymmetric, what means: $\frac{\partial}{\partial \theta} = 0$. Thus, these equations can be written:

$$W_r \frac{\partial W_x}{\partial r} + W_x \frac{\partial W_x}{\partial x} = -\frac{1}{\rho} \frac{\partial p}{\partial x} \quad (2.5)$$

$$W_r \frac{\partial W_r}{\partial r} + W_x \frac{\partial W_r}{\partial x} - \frac{W_\theta^2}{r} - 2\omega W_\theta - \omega^2 r = -\frac{1}{\rho} \frac{\partial p}{\partial r} \quad (2.6)$$

$$W_r \frac{\partial W_\theta}{\partial r} + W_x \frac{\partial W_\theta}{\partial x} + \frac{W_\theta W_r}{r} + 2\omega W_r = 0 \quad (2.7)$$

These equations are not practical to use in each calculation node described in the previous paragraph. In practical cases, most of the quasi-normal stations indeed have a x - and r - component. Hence, the pressure gradients calculated along a station have a x - and r - component as well, what means that equations (2.5) and (2.6) cannot be used separately.

2.1.3 Practical use of the equation of motion

In practical cases, the equation of motion is projected on the direction of the streamlines. By this way, one equation only describes the fluid motion in the meridionnal direction. In the streamline curvature method, the equation of motion is applied to a fluid particle at the intersection of a station i and a streamline j . The meridionnal velocity determines the local direction of the streamline j . The equation of motion is then projected in this direction, and the pressure gradients are calculated along the direction of the station i . An example of a calculation node is plotted Figure 16.

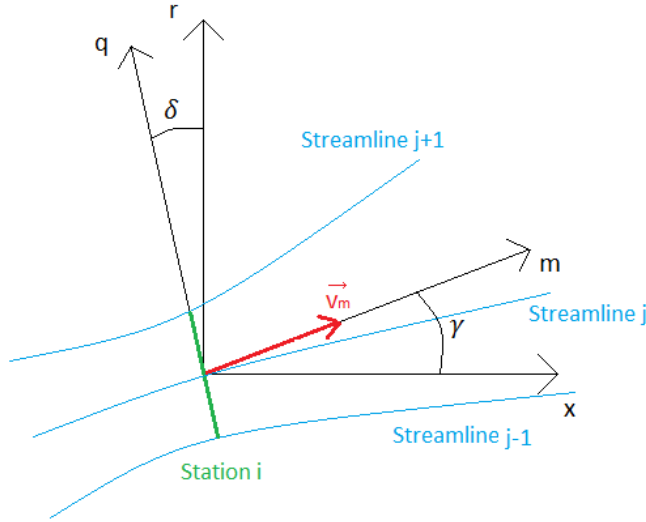


Figure 16: Basis for the streamline curvature

The quasi-normal direction q is defined with the angle $\delta = (\vec{r}, \vec{q})$, and the meridional direction m is defined with the angle $\gamma = (\vec{x}, \vec{m})$. The pressure gradients in direction q can be given by:

$$\frac{1}{\rho} \frac{dp}{dq} = \frac{v_\theta^2}{r} \cos(\delta) - \frac{v_m^2}{r_c} \cos(\gamma - \delta) - v_m \frac{dv_m}{dm} \sin(\gamma - \delta) \quad (2.8)$$

The circumferential velocity v_θ is the flow velocity component in the (x, θ) -plane, and the meridional velocity v_m is the flow velocity component in the (x, r) -plane, so that $v_m \vec{m} = v_x \vec{x} + v_r \vec{r}$. r_c is the local curvature radius of the streamline.

The pressure gradient in the q -direction can be written: $\frac{dp}{dq} = \frac{dp}{dr} \frac{dr}{dq} + \frac{dp}{dm} \frac{dm}{dq}$, what means:

$$\frac{1}{\rho} \left[\frac{dp}{dr} \cos(\delta) + \frac{dp}{dm} \sin(\gamma - \delta) \right] = \frac{v_\theta^2}{r} \cos(\delta) - \frac{v_m^2}{r_c} \cos(\gamma - \delta) - v_m \frac{dv_m}{dm} \sin(\gamma - \delta) \quad (2.9)$$

The angle $\gamma - \delta$ is close to zero for axial turbines. Thus, to first order the terms $\sin(\gamma - \delta)$ can be neglected. When the stations are significantly apart from each other, the terms $\frac{dp}{dm}$ and $\frac{dv_m}{dm}$ cannot be calculated precisely. Hence, the equation of motion used in practical cases is:

$$\frac{1}{\rho} \frac{dp}{dr} = \frac{v_\theta^2}{r} \cos(\delta) - \frac{v_m^2}{r_c} \cos(\gamma - \delta) \quad (2.10)$$

As regards the academic case of a cylindrical streamtube, with an axial flow velocity through a normal station, we have: $\gamma = 0$, $\delta = 0$, $v_r = 0$, and $r_c \rightarrow \infty$. Thus, the equation of motion is:

$$\frac{1}{\rho} \frac{dp}{dr} = \frac{v_\theta^2}{r} \quad (2.11)$$

Equation (2.11) is consistent with equation (2.6), where $W_r = v_r = 0$.

Equation (2.10), called radial equilibrium equation, is especially useful in the streamline curvature method, because it provides a radial distribution of the pressure in the turbine duct. Its use will be described in paragraph 2.2.3.

2.2 Program Code SLC4T

The program code SLC4T (StreamLine Curvature for Turbine), implemented by the DLR, can be used for axial turbines and uses the Streamline Curvature Throughflow Method. The flow is supposed axisymmetric, which means that all quantities are replaced by their mean value in the circumferential direction.

2.2.1 Input quantities

First of all the channel geometry and blade geometry is given. An example of the HWSS-Turbine, a 2-stages turbine, is given Figure 17.

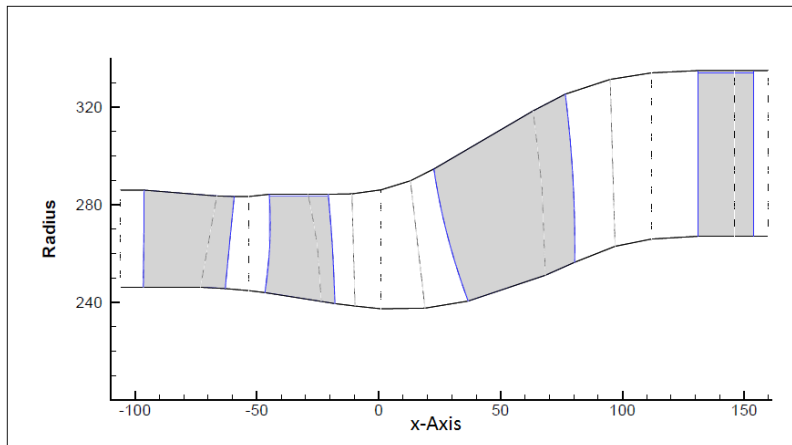


Figure 17: HWSS-Turbine – Position of the stations

This turbine consists of a 1-stage High Pressure Turbine, and of the first stage of a Low Pressure Turbine. Many stations are set along the axial direction. The turbine inlet, turbine outlet, and each blade inlet, blade outlet, and throat are described by a station. Other stations can be set through two consecutive blade rows. The stations are more or less perpendicular to the streamlines. Since the blade leading edge and blade trailing edge form generally no straight lines, the stations are not always straight either. Cooling air can be discharged in the flow at a certain station. A summary of the inlet quantities is shown Figure 18.

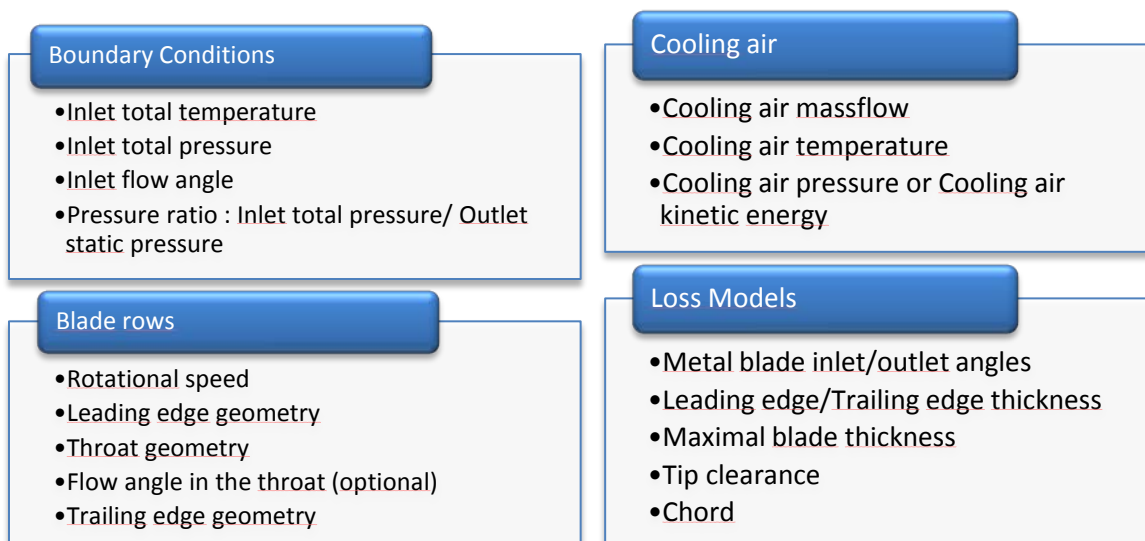


Figure 18: SLC4T inlet quantities

2.2.2 1D-calculation of the airflow

2.2.2.1 Definition of the inlet boundary conditions

In order to initialize the calculation, the static pressure at each blade outlet is calculated in several iterations from the inlet station to the outlet station, until the massflow calculated in each station converges. The outlet static pressure is set as outlet boundary condition. The inlet quantities set as boundary conditions are the total temperature, total pressure, and inlet flow angle. Thanks to the massflow conservation, the other thermodynamic quantities will be able to be calculated.

2.2.2.2 Calculation of the aero-thermodynamic properties at a control surface

In order to calculate the aero-thermodynamic properties over the channel, two different calculations can be performed, depending on whether the control surface is in a blade or not. In non-bladed control surfaces, the aero-thermodynamic properties are calculated according to the classical conservation laws, as described in Appendix A1. In bladed-control surfaces, the massflow conservation through the blade row is used from the throat to the blade trailing edge. The following conservation laws and correlations are used:

- *Rothalpy conservation*: the energy is conserved in the rotational system. When cooling air is discharged, the corresponding energy has to be added.
- *Outlet angle correlation*: To calculate the outlet flow angle, the Cosinus-Law is used in a control surface defined from the throat station to the trailing edge station. This correlation is detailed in Appendix A2.
- *Blade loss correlations*: It is very difficult to estimate the blade loss with formal equations. Thus, correlations published in the literature have been used. Usually the authors distinguish two types of blade losses. The main part consists in profile loss that can be minimized as the flow is adapted to the blade profiles. The second part, more difficult to identify, is called secondary loss. Many correlations have been implemented, with the help of experimental results, in order to model this secondary loss. The blade losses are calculated with the correlations established by Ainley-Mathiesen [4], Dunham-Came [5], revised by Kacker and Okapuu [6]. The equations used by Ivan Carlsson [7] are implemented in the program code SLC4T. The secondary losses in blade rows in the span direction are used according to the work of Benner [8].

2.2.2.3 Iteration

A distribution of the static pressure in the blade outlets is provided to initialize the iterative massflow calculations. The iterations are going on until the massflow in each station of the turbine has reached the target massflow, which is the mean of all the calculated massflows. A relaxation factor rx , is used to calculate the pressure from iteration k to iteration $k + 1$: $p_{k+1} = p_k + rx \cdot \Delta p_k$. In most cases $rx = 0.5$ gives a satisfying massflow initialization. An example of the pressure distribution in each blade outlet is given Figure 19. The corresponding massflow calculation is plotted Figure 20.

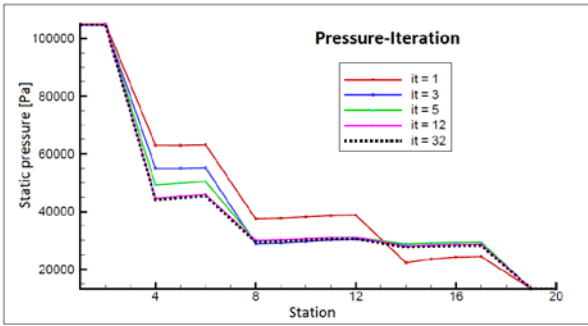


Figure 19: Pressure Iteration

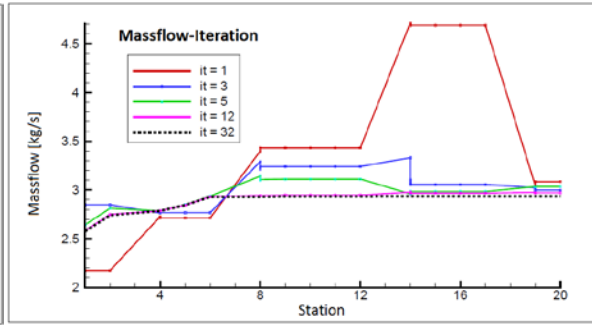


Figure 20: Massflow Iteration (Cooling air: station 2, 4, 5, 6, 9)

The turbine inlet and outlet pressure are set as fixed boundary conditions. The pressure distribution through the turbine rests on the fact that the pressure decreases over each rotor. In 32 iterations the massflow converges, what means that the massflow difference is lower than 0.2 %.

2.2.3 2D-calculation of the meridional flow

As seen previously, the 1D-calculation considers the whole annulus as one streamtube. For the 2D-calculation, the annulus is divided into several streamtubes ; each of them is delimited by two consecutive streamlines. The 2D-calculation rests on 1D-calculations in each streamtube. Then the streamlines are coupled thanks to a radial equilibrium between all the streamlines. The calculation chain is presented Figure 21.

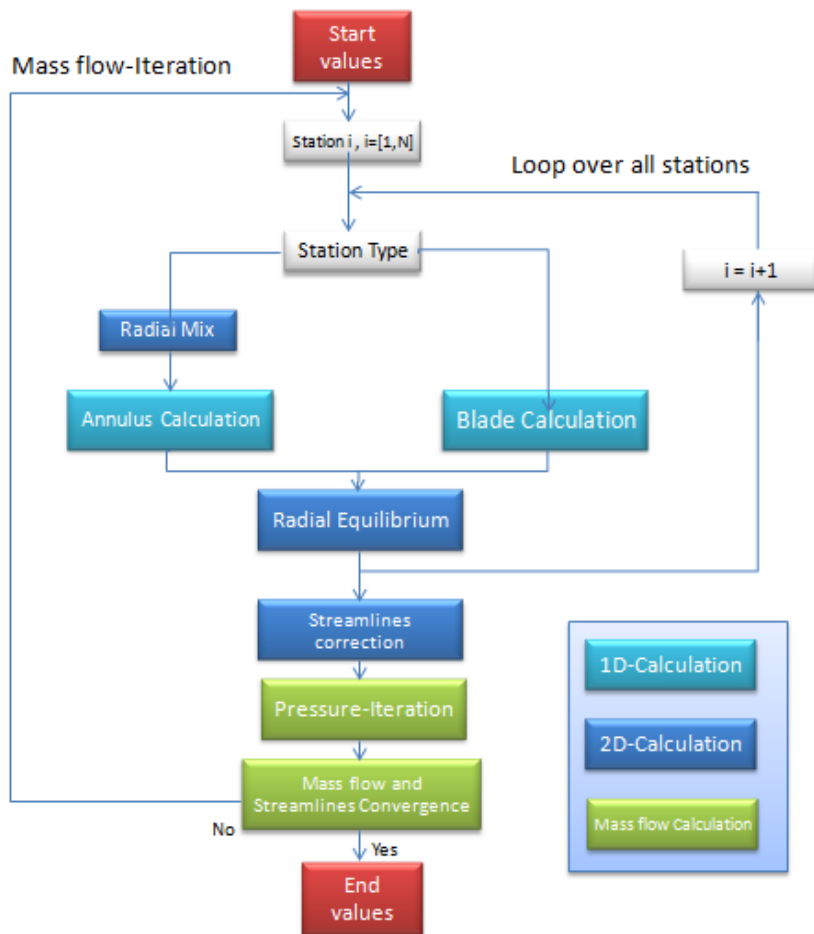


Figure 21: SLC4T Computation loop

- *Start values*: The position of the streamlines has to be initialized. At first the streamlines are set in the annulus according to a regular geometric repartition. The aero-thermodynamic flow properties are initialized in each node with the results provided by the 1D-calculation.
- *Radial Mixing*: The radial mixing is used only in non-bladed control surfaces, because the loss models used for bladed control surfaces provide a radial distribution of the flow properties. We make the assumption that the total pressure, total enthalpy and angular momentum are mixed in the radial direction because of the radial turbulence. The rate of entropy variation is used to quantify the turbulence. Thus, the turbulence factor in the radial direction is defined for station i , streamline j , by : $Tu_r = mix \cdot \frac{S_{j,i-1} - S_{min,i-2}}{S_{min,i-2}}$. In most cases the minimal entropy $S_{min,i-2}$ is to be found on the mean line of the annulus. Thanks to the mixing factor mix , the turbulence factor can be adapted for each test case.
- *Annulus Calculation/Blade Calculation*: the flow properties are computed in a loop over all streamtubes. In each streamtube the equations and correlations reported in paragraph 2.2.2.2 are implemented.
- *Radial Equilibrium*: The equation of motion (2.10), described in paragraph 2.1.3, provides a relation between the flow velocity and the pressure gradients along a radial direction. Therefore it is called radial equilibrium equation. Thanks to this equation, the static pressure in each streamtube is calculated from the mean static pressure. From the radial equilibrium equation, a pressure distribution can be provided in the turbine duct. However the calculated static pressure is not directly used, but it is adjusted with the help of a relaxation factor. This is done by a loop over each streamtube, and then by a second loop over all stations.
- *Streamlines correction*: the position of all the streamlines is updated with relaxation, so as to ensure equal massflow in each streamtube. The updated annular surface $A_{i,j\ new}$ in station i , streamline j , is given by : $A_{i,j\ new} = \frac{\dot{m}_{i,T}}{\dot{m}_{i,j}} A_{i,j}$, where $\dot{m}_{i,T}$ is the target massflow and $\dot{m}_{i,j}$ is the current massflow. Thus, some geometric quantities are changed (e.g. the curvature). The aero-thermodynamic properties are interpolated from the previous nodes to the updated ones.
- *Pressure-Iteration*: This procedure consists in a loop over all blade trailing edge stations. The static pressures in the meanline are iteratively modified, until all massflows have reached the corresponding target massflows as shown in paragraph 2.2.2.3. The turbine inlet total pressure and turbine outlet static pressure are boundary conditions.
- *Massflow and streamline convergence*: As long as the target massflows are not reached in all stations, the computation goes on, and the whole computation process is repeated. When the expected massflows are reached, the program stops. The convergence is reached with a precision of 0.2 %.

3 Integration of the Program Code SLC4T

The activities lead by DLR during the internship consisted in the validation and integration of the program code SLC4T previously described. The program code SLC4T has been validated by comparing results with those provided by 3D-CFD computations. Then the program code SLC4T has been integrated in the turbine pre-design chain that is presented paragraph 1.1.2. It has been used for the creation of turbine maps and for the optimization of the annulus contour.

3.1 Task 1 - Calibration and validation of SLC4T-Calculations

In order to estimate the quality of the results provided by SLC4T, a validation test has been performed by comparing the SLC4T results with 3D-CFD results. The test case is a 1 stage high pressure turbine called the Fox-Turbine. An overview of the Fox-Turbine is given Figure 22.

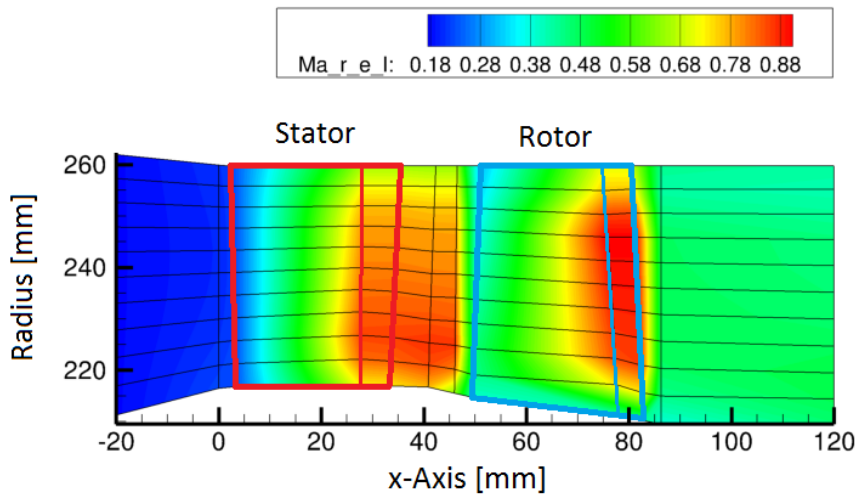


Figure 22: Fox-Turbine - SLC4T - Relative Mach number

3.1.1 SLC4T/3D-CFD Computation – Global flow properties

Two 3D-CFD computations have been performed on the Fox-Turbine - one with cooling air and the other one without any cooling air - with the help of the program code TRACE, developed by the DLR. The computation input data are summed up in the Table 1.

Gas Parameters		
cp [J/kg/K]		1322.2
r_gas [J/kg/K]		244.6
Boundary Conditions		
Inlet Total Pressure [Bar]		32.17
Inlet Total Temperature [K]		1736
Pt_Inlet / Ps_Outlet		2.206
Mecanical Parameters	Blades number	Rotational speed [RPM]
Stator 1	40	0
Rotor 1	60	14500

Table 1: Fox-Turbine – SLC4T/TRACE - Input Data

The SLC4T and 3D-CFD results are summed up in Table 2 (No Cooling) and Table 3 (With Cooling). In both cases, the relative error % *error* is calculated: $\% \text{ error} = \frac{SLC4T - CFD}{CFD} * 100$.

Thermodynamic Quantities	SLC4T No cooling	CFD No Cooling	% Error
Pt_Inlet / Ps_Outlet	2.205	2.205	0.00
Pt_Inlet / Pt_Outlet	1.969	1.993	-1.19
m_Inlet [kg/s]	76.53	77.56	-1.33
m_Outlet [kg/s]	76.53	77.57	-1.34
Corrected massflow [kg/s*K ^{0.5} /Pa*10 ⁶]	991.2	1004.5	-1.33
Power [kW]	18033.2	19192.7	-6.04
Specific Work [J/kg]	235639	247436	-4.77
Isentropic Efficiency	0.872	0.902	-3.38
Turbine Outlet Total Temperature [K]	1558	1548	0.62

Table 2: Fox-Turbine - SLC4T/TRACE No Cooling - Output Data

Without any cooling, the massflow calculated by SLC4T is 1.3% lower than the massflow calculated by TRACE. The biggest difference concerns the power: the power calculated by SLC4T is 6% lower than the one calculated by TRACE. Since the massflow and the power calculated by SLC4T are both lower than those calculated by TRACE, the error on the specific work is reduced: the specific work *SW* indeed is defined by: $SW [J/kg] = \frac{Power [W]}{m_{outlet}[kg/s]}$. The isentropic efficiency η_{is} is defined by: $\eta_{is} = \frac{Power}{Isentropic Power}$. Since the power provided by SLC4T is lower than the one provided by TRACE, the isentropic efficiency provided by SLC4T is likewise lower than the one provided by TRACE.

In the case cooling air is discharged in the turbine annulus, several SLC4T computations have been performed, in order to describe the cooling air behavior as well as possible. A report about this study is given in paragraph 3.1.2. The results presented in Table 3 have been obtained with the SLC4T cooling air parameters that seem to be the most convenient.

Thermodynamic Quantities - TE 1 SS 1	SLC4T Cooling	CFD Cooling	% Error
Pt_Inlet / Ps_Outlet	2.206	2.206	0.00
Pt_Inlet / Pt_Outlet	1.942	1.980	-1.90
m_Inlet [kg/s]	71.47	69.08	3.46
m_Outlet [kg/s]	85.15	82.31	3.46
Corrected massflow [kg/s*K ^{0.5} /Pa*10 ⁶]	925.7	894.7	3.46
Power [kW]	17231.1	18040.0	-4.48
Specific Work [J/kg]	202355	219181	-7.68
Isentropic Efficiency	0.863	0.897	-3.85
Turbine Outlet Total Temperature [K]	1438	1424	1.00

Table 3: Fox-Turbine - SLC4T/TRACE With Cooling - Output Data

In the case of cooling, the massflow calculated by SLC4T is higher than the one calculated by TRACE. The gap indeed is +3.5%. However, the power calculated by SLC4T is lower than the one calculated by TRACE. Therefore the specific work provided by SLC4T is especially lower than the one provided by TRACE. The isentropic efficiency provided by SLC4T is 3.85% lower than the one provided by TRACE.

As a conclusion, the results provided by SLC4T are not reaching the highest precision, but the results are precise enough to provide a reliable trend. Furthermore the computation time of a SLC4T

computation is inferior to 1 second, whereas the computation time of the TRACE computation is about 11 hours. For turbine pre-design, it can be of interest to keep in mind the gaps that have been noticed between the SLC4T and TRACE computations. Therefore the errors on the computed aerothermodynamic quantities are summed up in Table 4. The other quantities are obtained from those presented in this Table.

Computed Quantities	No Cooling	Cooling	
Pressure Ratio	-1.19%	-1.90%	< 2%
Massflow	-1.34%	3.46%	< 5%
Power	-6.04%	-4.48%	< 7%
Outlet Temperature	0.62%	1.00%	

Table 4: Fox-Turbine - SLC4T/TRACE - Summary

3.1.2 Calibration of the air cooling parameters

The air cooling is an important factor for the mechanical life of the blade rows, especially in high pressure turbines. The combustion chamber raises indeed the air flow temperature up to 1736°C in the case of the Fox-Turbine. Discharging of coolant in the turbine modifies the air massflow. Although the streamline curvature theory is based on massflow conservation, discharging of coolant can be taken into consideration by SLC4T, according to the principle: $\dot{m} = \dot{m}_{in} + \dot{m}_{cool}$. In each quasi-normal station, the discharging of coolant can be simulated by SLC4T. The cooling air massflow and the cooling air temperature are given. The cooling air is subjected to different aerothermodynamic conditions, according to the place, where it is discharged. Therefore an indication is given about the cooling air kinetic energy. If the cooling air is injected in the direction of the main flow, as it is the case in the blade trailing edge, the kinetic energy is set to TRUE. On the opposite, the cooling air injected through the pressure side has no kinetic energy, because the cooling air is injected in the opposite direction to the main flow. A summary of the cooling air injection is given on Table 5.

Cooling Parameters			
	m_cool/m_inlet [%]	T_cool [K]	Kinetic Energy (bool)
Stator 1			
Pressure Side	2.62	830	0
Suction Side	3.67	830	1
Tip Clearance	0.00	830	0
Trailing Edge	3.67	830	1
Cavity	1.19	830	0
Rotor 1			
Pressure Side	3.05	830	0
Suction Side	2.54	830	1
Tip Clearance	0.00	830	0
Trailing Edge	2.41	830	1
Cavity	0.00	830	0

Table 5: Fox-Turbine - Cooling Parameters

The effect of the cooling air on the flow can be seen in the entropy variations over the turbine. The cooling air reduces indeed the thermal agitation. Hence the cooling air is responsible for entropy decrease. The entropy variation is plotted in Figure 23 for several cooling air injections.

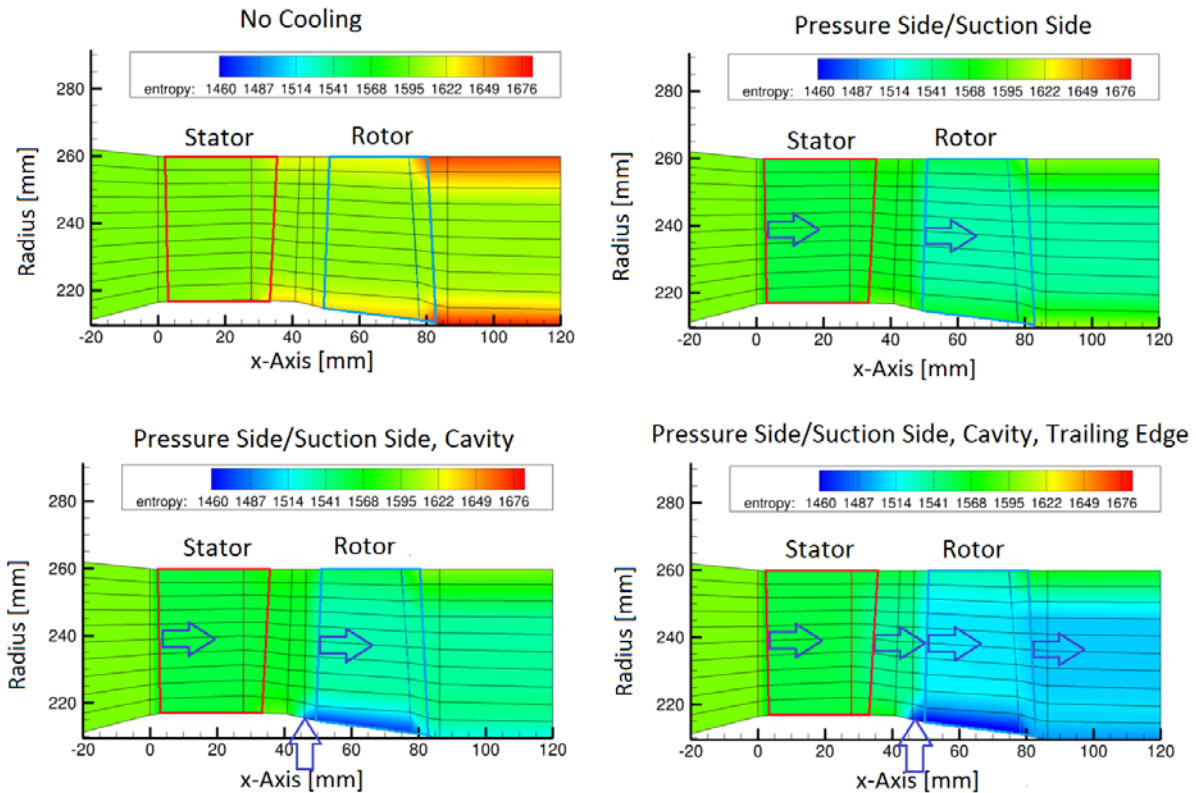


Figure 23: Fox-Turbine - Cooling air discharge

Without any cooling air, the entropy increases along the turbine duct. The rotor seems to increase significantly the thermal agitation in the hub and tip. The cooling air injected through the blades in the pressure side and suction side prevents the entropy increase that could be seen downstream of the rotor. Then the effect of the cavity in the hub, between the stator and the rotor is especially noticeable along the hub. Thus the entropy increase that could be seen along the hub is even replaced by a entropy decrease downstream of the rotor. Eventually, the cooling air injected through the trailing edge contributes to decreasing the entropy along the whole annulus radius. In case cooling air is injected through the rotor tip clearance, the entropy can decrease along the tip casing as well. By this way, the entropy decreases significantly along the turbine duct and the radial distribution of entropy is relatively regular.

In order to calibrate the cooling air behavior, several SLC4T computations have been performed with different kinetic energy values. Three cooling air configurations, described in Table 6 have been tested:

Kinetic Energy	Pressure Side	Suction Side	Tip Clearance	Trailing Edge	Cavity
TE1 SS1	0	1	0	1	0
TE1 SS0	0	0	0	1	0
TE0 SS0	0	0	0	0	0

Table 6: Fox-Turbine - Cooling air configurations

In the cases the cooling air is injected in a direction that does not fit the main flow direction, it seems reasonable to set the kinetic energy to FALSE. That concerns the pressure side, the tip clearance and the cavity. However when the cooling air is injected in the direction of the main flow, the cooling air

could be rapidly driven by the main flow. Therefore just after the injection, its velocity is those of the main flow. The cooling air kinetic energy should be set therefore to TRUE. In order to clarify these considerations, it could be of interest to determine which configuration provides the most convenient results. The relative error on the SLC4T results is plotted on Figure 24.

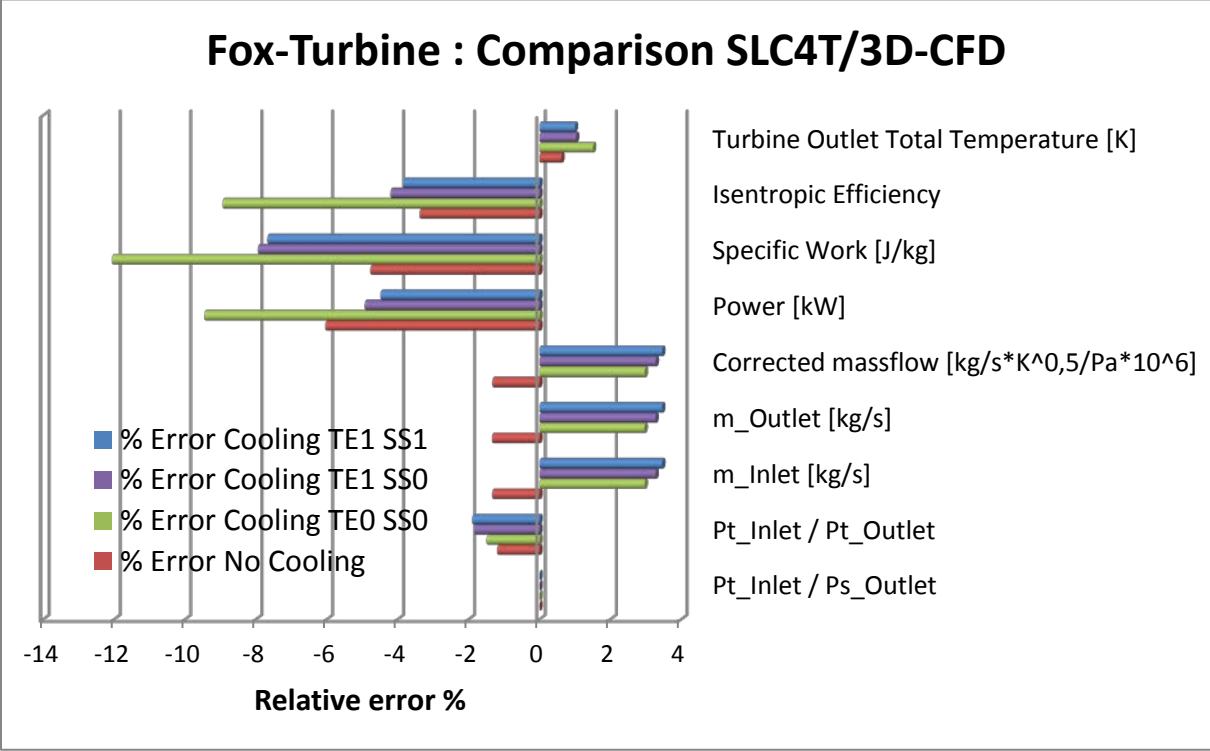


Figure 24: Fox-Turbine - Comparison SCL4T/TRACE

As seen previously in paragraph 3.1.1, the massflow calculated by SLC4T is about 3% higher than the one calculated by TRACE in the case of cooling. The slight difference between the massflows calculated for the cooling configurations TE1 SS1, TE1 SS0 and TE0 SS0 can be explained by the fact that a part of the main flow kinetic energy is used to drive the cooling air. The more kinetic energy the cooling air has when it is injected, the less energy the main flow uses to drive the cool air. Therefore the flow velocity and the massflow are higher, when the cooling air kinetic energy is high. Furthermore the more main flow energy is used to drive the cooling air, the less mechanical energy is provided by the main flow to the spool. Thus the power delivered to the spool is higher when the cooling air kinetic energy is high. The specific work and the isentropic efficiency are subjected to same considerations, because they are proportional to the power. Eventually the turbine outlet temperature is proportional to the outlet flow enthalpy. The higher the mechanical power, the more energy has been converted from the flow. Therefore the outlet temperature is lower, when the mechanical power is high.

It seems that the cooling configuration TE0 SS0 is not satisfying, because of too low mechanical power. However there is only little to choose between the TE1 SS0 and TE1 SS1 configuration. Thus it seems convenient to set the trailing edge cooling air kinetic energy to TRUE. If the suction side cooling air kinetic energy has to be set likewise to TRUE is left to the choice of the user. Regarding the cavity-, trailing edge-, and pressure side- cooling air, the physical sense would tend to set the kinetic energy to FALSE.

3.1.3 SLC4T/3D-CFD Computation – Local flow properties

Since the air cooling parameters have been calibrated by comparing the SLC4T results and TRACE results, it would be of interest to perform SLC4T computations with convenient cooling parameters and to compare the local distribution of the aero-thermodynamic parameters with the results provided by CFD computations. Thus the cooling configuration TE1 SS0 has been chosen for the SLC4T computations. The CFD computations are providing 3D results, whereas SLC4T is providing a mean value in the circumferential direction. Therefore the quantities computed by TRACE should have been averaged. The Mach number distribution provided by SLC4T and the mean Mach number provided by TRACE are plotted Figure 25 and Figure 26.

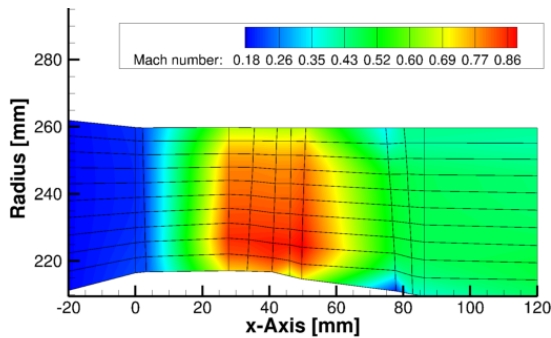


Figure 25: Fox-Turbine – SLC4T - Mach number

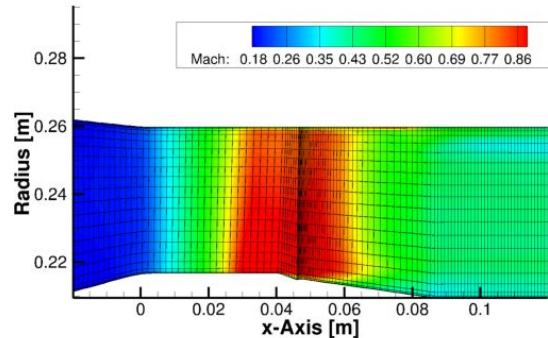


Figure 26: Fox-Turbine - TRACE - Mach number

The high flow deviation in the stator outlet induces a steep increase of the Mach number in the stator outlet. Regarding SLC4T, the calculation of the flow velocity in boundary layers is not obvious, since the streamlines are noticeably distant one another.

Figure 27 provides a distribution of the static temperature computed by SLC4T and Figure 28 provides a mean of the static temperature computed by TRACE.

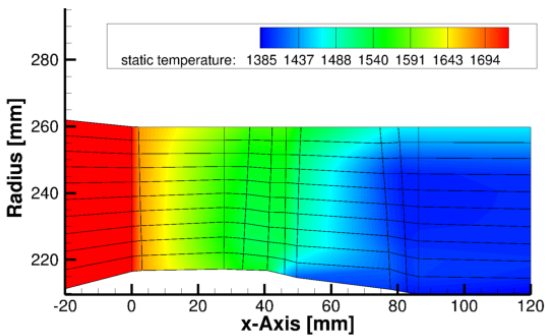


Figure 27: Fox-Turbine – SLC4T - Static temperature

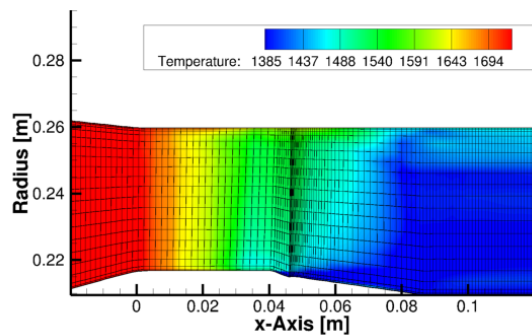


Figure 28: Fox-Turbine - TRACE - Static temperature

The temperature distribution is really similar for both computations. The fluid temperature decreases relatively regularly from the turbine inlet to the stator outlet. Then, the adjunction of cool air in the cavity, at $x = 45 \text{ mm}$, involves a significant decrease of the temperature.

Since SLC4T doesn't provide any information about the distribution of the flow properties in the circumferential direction, it is of interest to compare the circumferential velocity calculated by SLC4T in the S2-surface with the mean of the circumferential velocities computed by TRACE. The

circumferential velocity provided by SLC4T is plotted Figure 29 and the mean of the circumferential velocities computed by TRACE is plotted Figure 30.

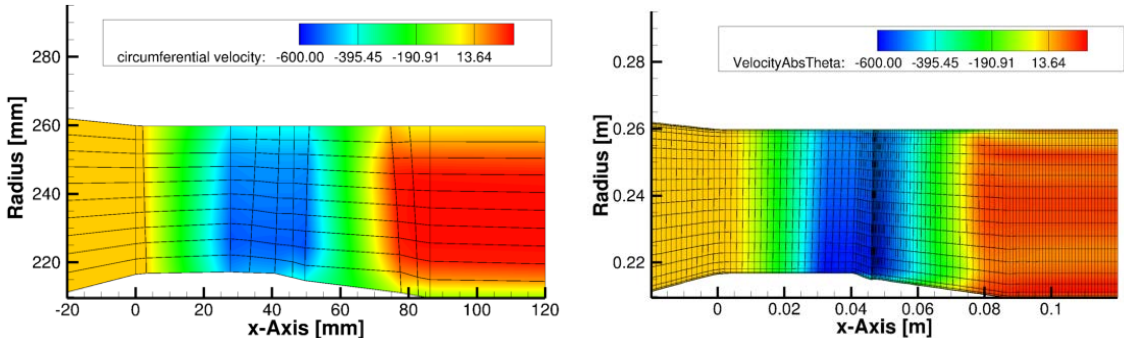


Figure 29: Fox-Turbine – SLC4T - Circumferential velocity Figure 30: Fox-Turbine - TRACE - Circumferential velocity

The comparison of Figure 29 and Figure 30 is all the more satisfying, than S2-computations are not especially high-achieving in the computation of circumferential quantities. These comparisons are really in favor of the validation of the program code SLC4T. The program code SLC4T is therefore of great interest for the turbine pre-design, because of the precision of the results, and the extremely low computation times. The convergence parameters are summarized in Table 7.

CPU-Time [s]	Iterations	Convergence Precision
0.0799	83	1.28E-05

Table 7: SLC4T - Computation time

83 iterations have been useful for the calculation of the Fox-Turbine, until equal massflow in each streamtube with a precision lower than 4.0E-4. Actually the maximal massflow difference between the streamtubes is only 1.28E-05. The computation time is lower than 0.1s. Regarding 3D-CFD, the computation time is about 11 hours. SLC4T seems to be a tool of great interest for the turbine pre-design.

3.2 Task 2 – Creation of turbine maps

3.2.1 First pre-design and turbine map

The first steps for the turbine pre-design are described in Figure 31.

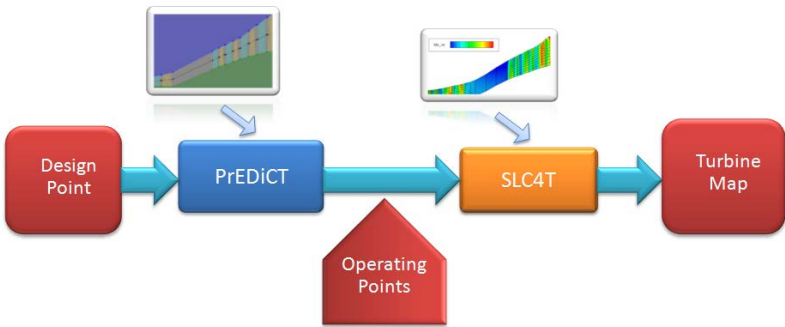


Figure 31: Process chain for Turbine Maps

At first the chosen design point leads to a 1D pre-design performed thanks to the program code PrEDICT. The output file is a .xml file that contains the flow quantities for each blade row. The flow

properties are calculated along the channel mean line, and are extended in several surfaces from the hub to the tip. By this way a radial distribution of the flow properties is provided. The main structure of the PrEDiCT output file is given Figure 32.

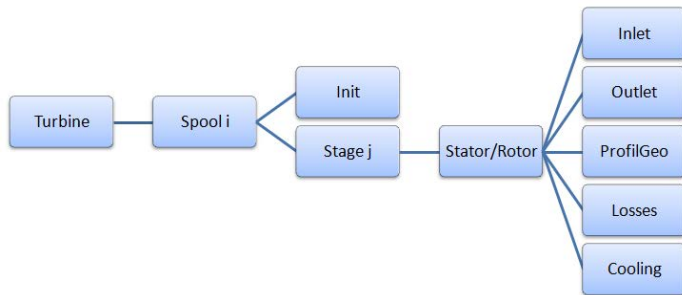


Figure 32: PrEDiCT output file structure

The PrEDiCT output file has to be converted in a SLC4T input file. The geometry of the turbine, as well as the aero-thermodynamic boundary conditions that suit to the chosen design point, the loss parameters, and the cooling properties have to be read from the PrEDiCT output file and written in the SLC4T input file. Thus the S2-computation can be run automatically. The aero-thermodynamic quantities calculated in each node can then be plotted. By this way an overview of the flow properties through the turbine is provided for a given operating point. An example of the 5-stages TATT-Turbine designed by PrEDiCT is given Figure 33. The 2D-flow calculated by SLC4T at the design point is plotted Figure 34. The design point parameters are described on Table 8.

Pt _{in}	Tt _{in}	Alpha _{in}	Cp	R	Pt _{in} /Ps _{out}	RPM S1	RPM S2
[Bar]	[K]	[deg]	[J/kg/K]	[J/kg/K]	[-]	[RPM]	[RPM]
15	1690	0	1213.49	285.42	21.953	12000	-5000

Table 8: TATT-5S-Turbine : Design Point

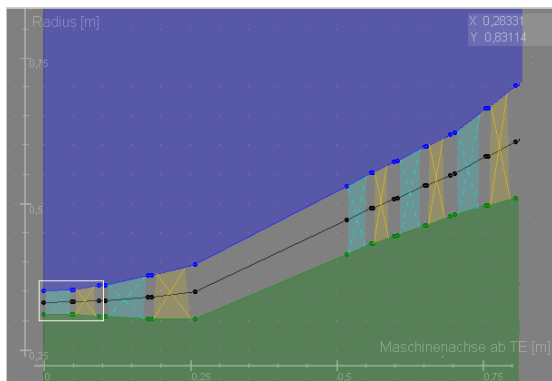


Figure 33: TATT-5S-Turbine - PrEDiCT

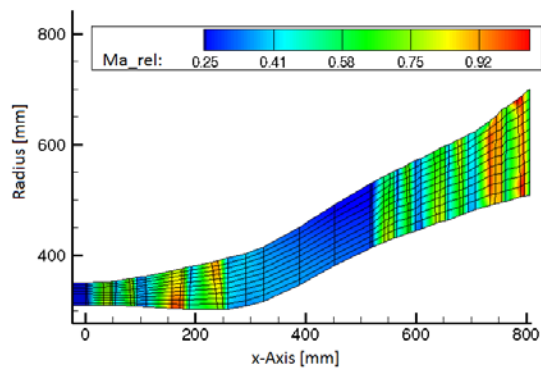


Figure 34: TATT-5S-Turbine - SLC4T

In order to plot a turbine map, it is necessary to run SLC4T computations for a large number of operating points. These operating points can be defined automatically in the SLC4T input file. Thanks to its high speed of calculation, SLC4T is able to compute 100 operating points with a CPU-Time lower than 20s by using a standard PC. The precision of 2D-calculations does not reach the one of 3D-CFD calculations, but the high speed of calculation is of great interest for such applications. The value ranges for the spool rotational speed and for the pressure ratio can be adjusted per hand. The defined operating points are then transferred in the SLC4T input file thanks to a program called Operating Points Generator. The operating points are computed by SLC4T and the flow properties

useful for the generation of turbine maps are then saved in a file, which is the input file for a Map Visualization Tool that is able to plot turbine maps. The detail of the implementation is to be found in the next paragraph 3.2.2

3.2.2 Implementation

The detail of the part of the chain described previously in paragraph 3.2.1 is given on Figure 35.

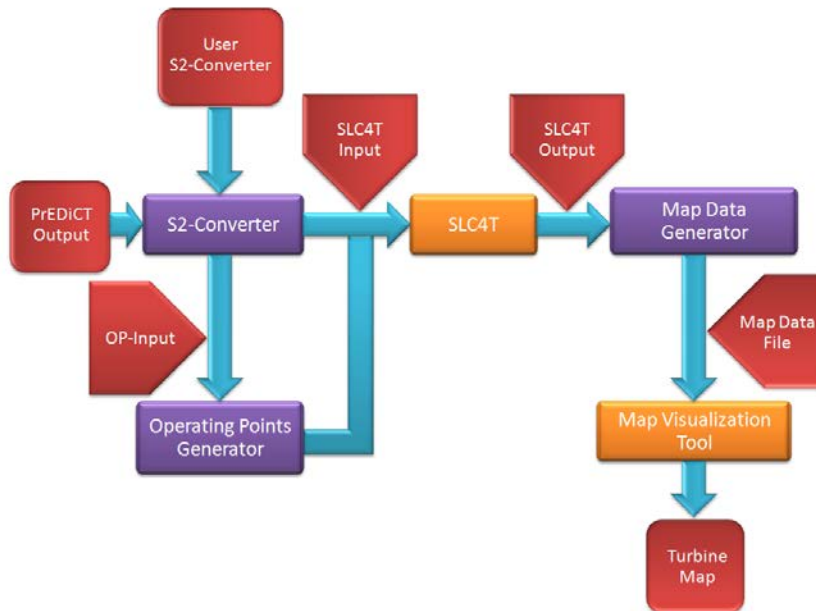


Figure 35: Process chain for Turbine Maps - Implementation

- S2-Converter*: The 1D pre-design provided by PrEDiCT is saved in the *PrEDiCT Output* file in .xml format. The *S2-Converter* is supposed to catch the useful data and to generate automatically a *SLC4T input* file. With the file *User S2-Converter*, the user can choose to catch the PrEDiCT Output of the whole turbine or of one spool only. The whole turbine can therefore be computed by SLC4T in order to get an overview of the flow at the design point. Each spool separately can be computed so as to plot the corresponding turbine maps.
- Operating Points Generator*: In order to prepare a turbine map, the *S2-converter* can define range values of the spool rotational speed and of the pressure ratios that could be suitable for the design point. Thus, the range values of the turbine map are defined in the *Operating Points Generator* input file, called *OP-Input*. Thanks to the program *Operating Points Generator*, each operating point is written in the *SLC4T Input* file. Thus, the *SLC4T Input* file contains the aero-thermodynamic boundary conditions that suit for the turbine map of the selected spool. Then, the program code SLC4T can calculate the flow properties over the turbine for each operating point.
- MapDataGenerator*: The flow properties in each calculation node and the global properties of the turbine are saved in *SLC4T Output* files. The global quantities useful for the generation of turbine maps (massflow, rotational speed, efficiency) are then transferred in a *Map Data File* in .mea format, thanks to the program *MapDataGenerator*. The Map Data File can be read by the *MapVisualizationTool*, which plots the expected turbine map.

3.2.3 Geometric design of Inter Turbine Ducts (ITD)

When turbines consist of several spools, the fluid flows from a high-pressure turbine to a low-pressure turbine through a not bladed duct called ITD (Inter Turbine Duct). In the early steps of the turbine pre-design, the ITD cannot be precisely designed. Thus, a high pressure turbine and a low pressure turbine are simply linked with a linear segment. When the turbine geometry is converted from PrEDiCT Output into SLC4T Input, it is desirable to define some quasi-normal stations along the ITD, so that the ITD geometry could be well adapted to the flow. The ITD geometry is no more designed with a linear-segment but has been replaced by a spline function. An example of ITD designed with a linear segment and with a spline function is given Figure 36 and Figure 37.

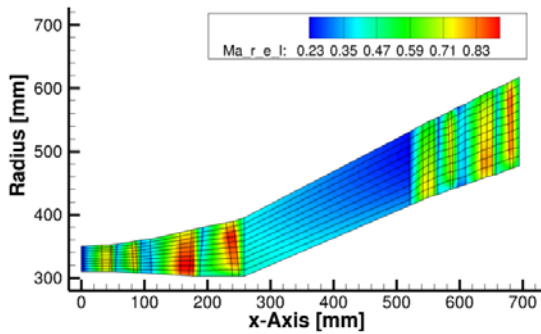


Figure 36: TATT-5S-Turbine - Linear ITD

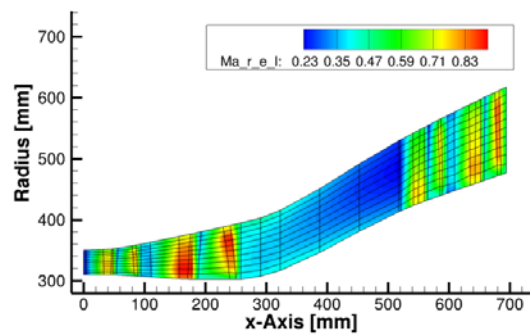


Figure 37: TATT-5S-Turbine - Spline ITD

The ITD design parameters provided by the program code PrEDiCT are used to determine the number and the position of the ITD quasi-normal stations. Thanks to the spline function, the ITD geometry is more adapted to the flow. Although the program code SLC4T doesn't calculate detachments, it is obvious that the ITD designed with the spline function is more appropriate to prevent detachments. Moreover in some cases the program code SLC4T doesn't converge because of too high annulus contour angles, for instance between the high pressure turbine and the ITD. The spline function is therefore of great interest.

3.2.3.1 Mathematical principle of the spline function

With the geometrical data of the last High Pressure Turbine rotor and the first Low Pressure Turbine stator, a spline function based on a polynomial of degree three can be determined, in order to define the ITD. Figure 38 explains how the spline function has been implemented.

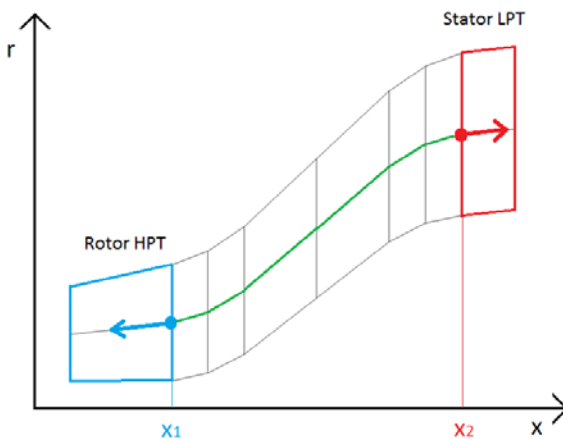


Figure 38: Principle of the spline interpolation

The mean line of the ITD is designed with a polynomial of degree three, what means that the ITD mean line can be defined by $(a, b, c, d) \in R^4$, so that:

$$r_m(x) = ax^3 + bx^2 + cx + d \quad (3.1)$$

The (a, b, c, d) coefficients can be determined with 4 boundary conditions: $r_m(x_1)$, $\frac{dr_m}{dx}(x_1)$ in the ITD inlet and $r_m(x_2)$, $\frac{dr_m}{dx}(x_2)$ in the ITD outlet.

This leads to the linear system:

$$A \cdot C = R \quad (3.2)$$

$$\text{With } = \begin{bmatrix} x_1^3 & x_1^2 & x_1 & 1 \\ x_2^3 & x_2^2 & x_2 & 1 \\ 3x_1^2 & 2x_1 & 1 & 0 \\ 3x_2^2 & 2x_2 & 1 & 0 \end{bmatrix}; C = \begin{bmatrix} a \\ b \\ c \\ d \end{bmatrix}; R = \begin{bmatrix} r_m(x_1) \\ r_m(x_2) \\ r_m'(x_1) \\ r_m'(x_2) \end{bmatrix}.$$

If $x_1 \neq x_2$, the matrix A^{-1} exists and the vector C is determined by $C = A^{-1}R$. Thus, the coefficients of the polynomial are determined and the spline function is known. In order to use the spline function in practical cases, it is necessary to set the boundary conditions, to determine which ITD-points are going to be calculated with the spline function, and to extend the mean ITD-line from the hub to the tip casing.

3.2.3.2 Implementation of the spline function

- *Set the boundary conditions:* the ITD inlet and outlet correspond to the last rotor of the high pressure turbine and to the first stator of the low pressure turbine. The inlet mean position $(x_1, r_m(x_1))$ and outlet mean position $(x_2, r_m(x_2))$ are given by a mean of the hub and tip position. The gradient function is calculated for the hub and the tip by left finite difference in the high pressure rotor and by right finite difference in the low pressure stator. Then, the hub and tip gradient functions are averaged and provide thus the gradient function on the mean line. By this way the 4 boundary conditions $r_m(x_1)$, $r_m(x_2)$, $r_m'(x_1)$, $r_m'(x_2)$ are defined.
- *Calculation of the mean line with the spline function:* according to the previous mathematical development, the (a, b, c, d) coefficients are calculated. By this way, the spline function $r_m(x) = ax^3 + bx^2 + cx + d$ is known.
- *Definition of the ITD hub and tip position:* The ITD mean line can be provided thanks to the spline function. The hub and tip position can be deduced from the mean line position, thanks to the ITD quasi-normal height. At first the quasi-normal height h_{in} and h_{out} are calculated in the ITD inlet and outlet. Then the quasi-normal height along the ITD $h(x)$ is calculated according to a linear interpolation. The tangential direction of the quasi-normal stations to be set along the ITD, will be given by the vector $\vec{t}(x)$. The vectors \vec{t}_{in} and \vec{t}_{out} are calculated in the ITD inlet and outlet. Then the tangential vector $\vec{t}(x)$ is calculated according to a linear interpolation between \vec{t}_{in} and \vec{t}_{out} .

- *Choice of the x-positions of the points calculated by the spline*: the number of ITD points that have to be calculated depends on the global ITD geometry. The general ITD geometry is characterized by its expansion, its longitudinal stretching and its radial deviation. These parameters are summed up in Table 9.

Expansion	Longitudinal stretching	Radial deviation
$\frac{A_{out}}{A_{in}}$	$\frac{L}{h_{in}}$	$\frac{r_{m_{out}} - r_{m_{in}}}{L}$

Table 9: ITD parameters

In order to determine the number of points that have to be calculated with the spline function, a correlation has been defined with these geometrical parameters. n_{in} points will be chosen to set the ITD inlet geometry, n_{out} points will describe the ITD outlet geometry, and n_{duct} will describe the duct itself. Hence the ITD geometry will be defined thanks n_{ITD} points:

$$n_{ITD} = n_{in} + n_{duct} + n_{out}. \quad (3.3)$$

The number of points describing the duct itself should increase with the ITD longitudinal stretching $\frac{L}{h_{in}}$. The radial deviation $\frac{r_{m_{out}} - r_{m_{in}}}{L}$ has an influence to a less extent. Thus n_{duct} has been defined by:

$$n_{duct} = \text{Rounddown}\left(\frac{L}{h_{in}} * 0.9 * \left(\frac{r_{m_{out}} - r_{m_{in}}}{L} + 0.7\right)\right). \quad (3.4)$$

The spline function is then calculated from the ITD inlet to the ITD outlet with a regular pitch p_{duct} , so that:

$$p_{duct} = \frac{L}{n_{duct} + 1}. \quad (3.5)$$

As regards the ITD inlet/outlet, the number of points calculated with the spline function is determined by comparing the ITD radial deviation $\frac{r_{m_{out}} - r_{m_{in}}}{L}$ with the inlet/outlet local deviation $\frac{dr_m(x_{in,out})}{dx}$. The number of points has to grow with the difference between these two quantities. Thus a correlation has been defined:

$$n_{in/out} = \text{Rounddown}\left(2 * \left| \frac{dr_m(x_{in,out})}{dx} - \frac{r_{m_{out}} - r_{m_{in}}}{L} \right|\right). \quad (3.6)$$

In order to precise the ITD inlet/outlet geometry $n_{in/out}$ points are added in the inlet/outlet area with a regular pitch $p_{in/out}$, so that:

$$p_{in/out} = \frac{p_{duct}}{n_{in/out} + 1}. \quad (3.7)$$

Hence all the mean x -positions x_m of the quasi-normal stations are defined. Thanks to the spline function, the r -positions r_m of the mean line can be calculated.

- *Set the final quasi-normal stations:* Then, the geometry of the hub and tip can be set for all the ITD quasi-normal stations. Thus, the ITD geometry is defined by:

$$x_{hub} = x_m - \frac{h(x_m)}{2} (\vec{t}(x_m) \cdot \vec{x}) \quad (3.8)$$

$$x_{tip} = x_m + \frac{h(x_m)}{2} (\vec{t}(x_m) \cdot \vec{x}) \quad (3.9)$$

$$r_{hub} = x_m - \frac{h(x_m)}{2} (\vec{t}(x_m) \cdot \vec{r}) \quad (3.10)$$

$$r_{tip} = r_m + \frac{h(x_m)}{2} (\vec{t}(x_m) \cdot \vec{r}) \quad (3.11)$$

3.2.3.3 ITD test cases

The elaboration of the correlations has been performed with trial and errors, so as to design ITD as varied as possible. Different ITD have been tested for several combinations of the geometrical parameters $\frac{A_{out}}{A_{in}}$, $\frac{L}{h_{in}}$, and $\frac{r_{m_{out}} - r_{m_{in}}}{L}$. The limit values commonly used are summed up in Table 10.

A_out/A_in	L/h_in	delta_rm/L
1.5	2.5	0.38
2	4.9	0.65

Table 10: ITD Design parameters

A long ITD is plotted Figure 39. With $\frac{L}{h_{in}} = 4.9$ and $\frac{r_{m_{out}} - r_{m_{in}}}{L} = 0.38$ the deviation is low and the duct is long. An aggressive ITD is plotted Figure 40. With $\frac{L}{h_{in}} = 2.5$, and $\frac{r_{m_{out}} - r_{m_{in}}}{L} = 0.65$ the flow is strongly deviated through a short duct.

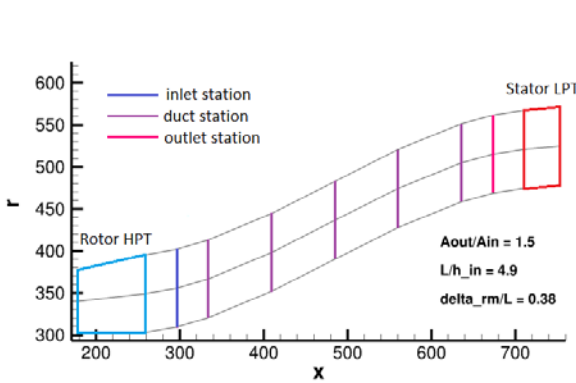


Figure 39: Long ITD interpolated by Spline function

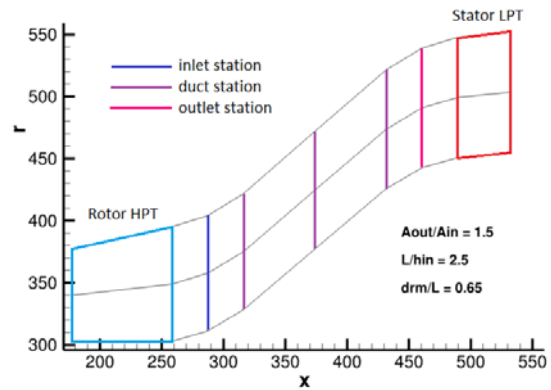


Figure 40: Aggressive ITD interpolated by Spline function

3.2.4 Interpolation of the quasi-normal stations

The 1D pre-design provided by PrEDiCT gives some information about blade row geometries. This information is useful to set the geometry of the quasi-normal stations in the leading edge and trailing edge of each blade row. In some cases, the geometry provided by PrEDiCT may have to be slightly modified, so as to ensure a high regularity of the annulus contours. Hence a spline interpolation can be used by the S2-converter, in order to provide an annulus contour as regular as possible. The geometry provided by PrEDiCT is used to create non-bladed stations. Then a spline function is calculated between two consecutive non-bladed stations for the hub and the tip. Thus, the leading edge station and trailing edge station geometry is determined thanks to the spline function.

3.2.5 Test case: TATT-5S-Turbine

The different steps of the turbine pre-design process have been conducted until the creation of turbine maps. The test case presented here is the TATT-5S-Turbine. This turbine is composed of a 2 stages high pressure turbine, and of a 3 stages low pressure turbine. Cooling air is injected in the high pressure turbine. An overview of the TATT-5S-Turbine is provided Figure 41.

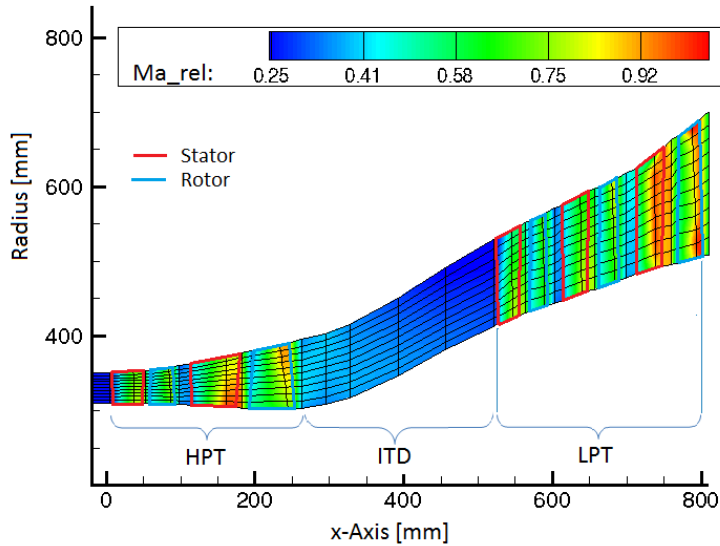


Figure 41: TATT-5S-Turbine : Relative Mach number

The High Pressure Turbine and the Low Pressure Turbine have been computed separately by SLC4T for several operating points, so as to cover the operating range of the pressure ratio and rotational speed. The thermodynamic quantities obtained for the design point are summarized in Table 11.

Thermodynamic Quantities	HPT	LPT	Whole Turbine
Pt_Inlet [Bar]	15.00	3.98	15.00
Tt_Inlet [K]	1690	1130	1690
Cooling massflow %	18.51	0	18.51
Pt_Inlet / Ps_Outlet	4.203	5.831	21.954
Ps_out [Bar]	3.569	0.683	0.683
Pt_Inlet / Pt_Outlet	3.742	4.827	17.602
Pt_out [Bar]	4.009	0.825	0.852
m_Inlet [kg/s]	49.87	57.29	49.93
m_Outlet [kg/s]	58.56	57.31	58.56
Corrected massflow [kg/s*K ^{0.5} /Pa*10 ⁶]	1366.7	4834.4	1368.3
Power [kW]	25533	21863	47396/48789
Specific Work [J/kg/K]	292.27	337.63	557.69
Isentropic Efficiency	0.817	0.906	0.881
Turbine Outlet Total Temperature [K]	1207	802	871

Table 11: TATT-5S-Turbine - SLC4T output data

If the adequacy of the HPT with the LPT is optimal, the following relations are respected:

$$p_{t\text{in}LPT} = p_{t\text{out}HPT} + \Delta p_{ITD}, \quad T_{t\text{in}LPT} = T_{t\text{out}HPT} + \Delta T_{ITD}, \quad T_{t\text{out}LPT} = T_{t\text{out}Whole\ Turbine},$$

$$\dot{m}_{\text{in}LPT} = \dot{m}_{\text{out}HPT}, \quad Power_{Whole\ Turbine} = Power_{LPT} + Power_{HPT}.$$

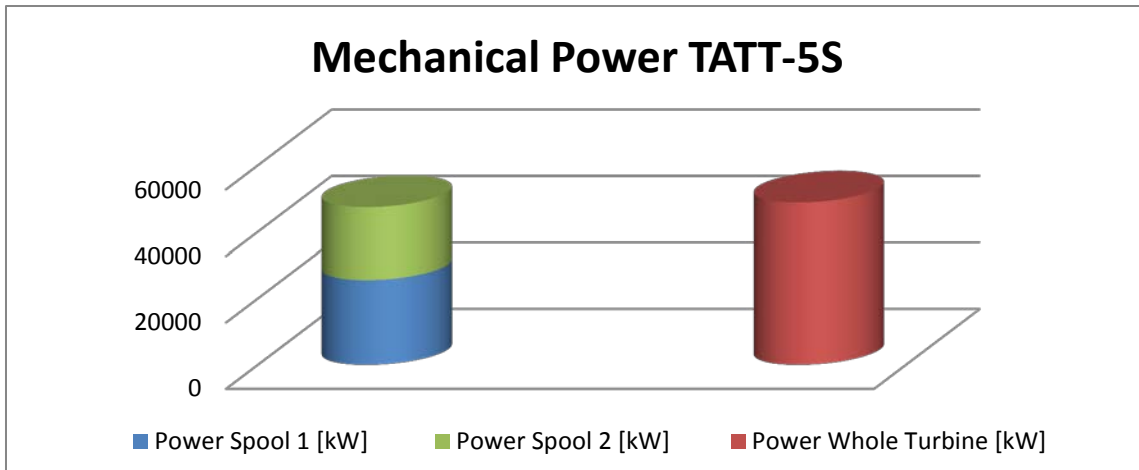


Figure 42: TATT-5S-Turbine - Mechanical power

The advantage of the turbine maps can be seen here: by coupling the LPT and HPT operating point, the behavior of the whole turbine can be improved.

The high pressure turbine map is given Figure 43.

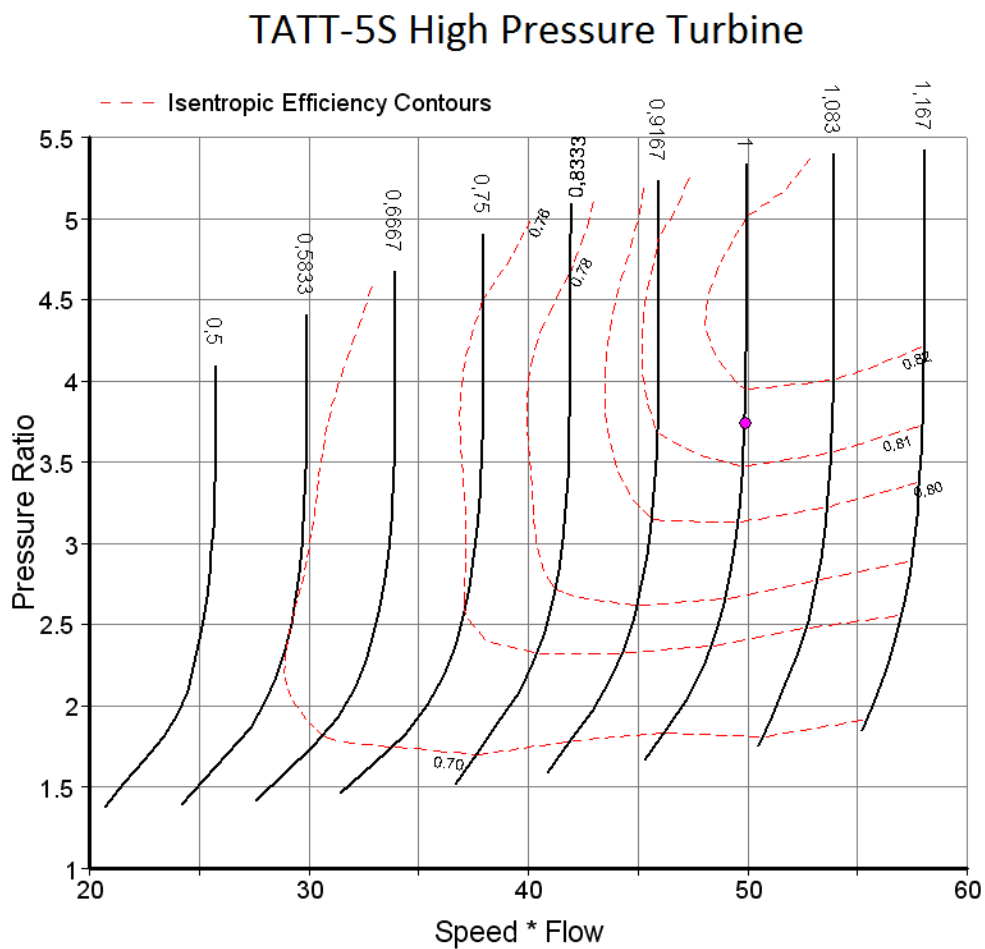


Figure 43: TATT-5S-Turbine Map - HPT - PressureRatio(Speed*Flow), Efficiency

The HPT has been designed by PrEDiCT for a pressure ratio $\frac{p_{t_{in}}}{p_{t_{out}}} = 3.742$. According to the turbine map, the highest efficiency is reached when the pressure ratio is about 4.5. Thus an iterative process can be lead, so that the low pressure turbine and the high pressure turbine design points are as optimal as possible as far as the efficiency is concerned. Furthermore it is necessary to make sure of the adequacy of the HPT outlet pressure to the LPT inlet pressure. Both for the HPT and for the LPT, the pressure ratio should match the expected mechanical power delivered to the spools. In the case of aircraft engines, the mechanical power of the LPT is determined by the fan and LP compressor, and the mechanical power of the HPT is determined by the HP compressor. Each compressor map has to be confronted to the corresponding turbine map, in order to find an optimal design point. In most cases, this matching leads to compromises.

The low pressure turbine map is given Figure 44. For many pressure ratios, especially for low pressure ratios, the massflow convergence has not been reached. The operating envelope of the low pressure turbine is therefore quite reduced around the design point.

TATT-5S Low Pressure Turbine

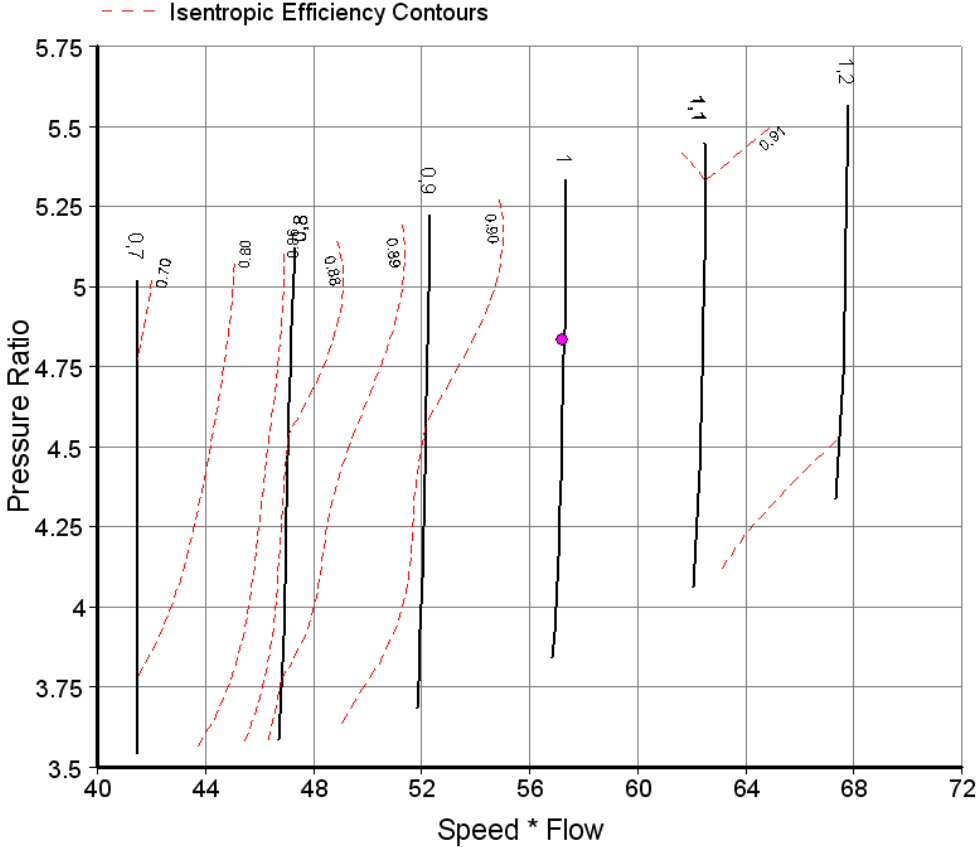


Figure 44: TATT-5S-Turbine Map - LPT - PressureRatio(Speed*Flow), Efficiency

The LPT has been designed by PrEDiCT for a pressure ratio $\frac{p_{t_{in}}}{p_{t_{out}}} = 4.827$. Although the convergence range is not wide, the current LPT seems quite convenient for this design point. The efficiency indeed $\eta_{is} = 0.906$ is satisfying.

3.3 Task 3 – Optimization of the annulus contour

As described in paragraph 1.2.4, once the blades rows have been designed and optimized, it is of interest to optimize the annulus contour. The program code SLC4T has been used also in order to optimize the annulus contour.

3.3.1 2D-computations and optimization of the annulus contour

At this step of the turbine pre-design, the annulus contour has not been modified, since the first 2S-flow computations have been performed in order to plot turbine maps. Therefore, the possibility of any optimization of the annulus contour would be of interest. The process chain implemented to optimize the annulus contour is presented Figure 45.

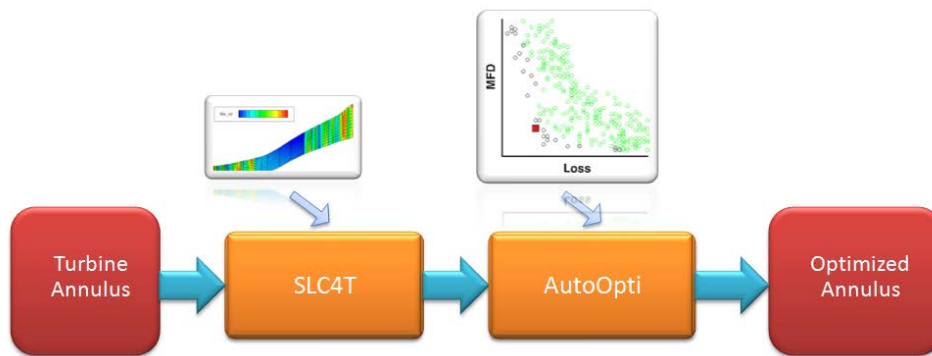


Figure 45: Process chain for annulus contour optimization

The geometrical blade parameters such as the leading edge and trailing edge angles, rotor tip clearance, and blade thickness, have an influence on the S2-flow computations. Therefore, the geometrical blade parameters are updated with those of the optimized blade rows. By this way, the optimized blade rows are integrated in the annulus contour. Thus, S2-flow computations can be performed so as to determine the optimal annulus contour. The optimization tool AutoOpti generates different annulus geometries, called members, with the help of genetic algorithms. A SLC4T computation is performed on each member, which provides the aero-thermodynamic properties of the member. Among these flow properties, the turbine efficiency is considered as a fitness function for the optimization process. The efficiency indeed constitutes one of the criteria to evaluate the pertinence of the member. According to the pertinence of the members, genetic algorithms aim to generate new members, whose fitness functions may be as close as possible to an optimum. The genetic algorithms are based on the assumption that the combination of members of high efficiency may generate members of high efficiency. When the improvement of the members is no more obvious, the optimization process has come to an end. The member that best meets the optimization criteria described in the fitness functions can be seen as the optimized turbine annulus.

3.3.2 Tool AutoOpti

AutoOpti is an optimization tool based on genetic algorithms. AutoOpti aims to minimize target quantities. In the case of turbine annulus contour optimization, an initial geometry of the turbine is set as initial member. The aero-thermodynamic losses constitute one of the target quantities that have to be minimized. The optimization consists in testing several members, whose geometry slightly varies from the initial member, until the target quantities have reached an optimum. A summary of the AutoOpti input and output is given Figure 46.

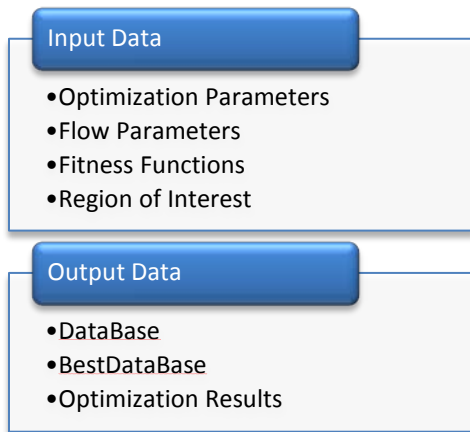


Figure 46: AutoOpti input/output data

- *Input Data*: The free geometric parameters that are going to vary, are called *OptimizationParameters*. The user defines the *OptimizationParameters* as well as their range of variation. AutoOpti is going to generate different members, in accordance with the ranges of variation defined for the free optimization parameters. AutoOpti executes the S2-computation and by this way tests the current member. The aero-thermodynamic properties useful for the optimization process, are defined by the user, and called *FlowParameters*. With the help of these *FlowParameters*, the target quantities, called *Fitness Functions*, are defined. In some cases, *FlowParameters* that are not seen as target functions have to be constrained in a range called *Region of Interest*. For instance, the value of the flow velocity is of little interest regarding the annulus optimization. However if the shape of the annulus contour implies very low velocities in the boundary layer, some detachments may occur, what has to be avoided. Therefore, the user can define flow velocity limit values thanks to a *Region of Interest*. If a *FlowParameter* is not in its *Region of Interest*, the corresponding member is downgraded.
- *Output Data*: All the members tested are graded in the *DataBase*. The best members are graded in the *BestDataBase*. The results of the S2-computations performed on each member can be saved. This large amount of data constitutes the *Optimization Results*. The user can define the number of members to be saved.

3.3.3 Implementation

In most cases the turbine is going to be optimized for its design point. Thus the aero-thermodynamic boundary conditions, as well as the spools' rotational speeds are set in the SLC4T input file, so as to reproduce the design point conditions. The SLC4T computation will be performed with these conditions for each member. A change of the annulus contour geometry can lead to angular contours, especially for wide *OptimizationParameters* ranges. Angular contours are not in favor of a regular flow, and can cause detachments. Therefore, the annulus contour regularity has to be checked. That is why a secondary program, called here *CheckGeometry* is integrated in the optimization process, so as to check the annulus contour geometry. The integration of the program code SLC4T in the optimization process can be seen Figure 47.

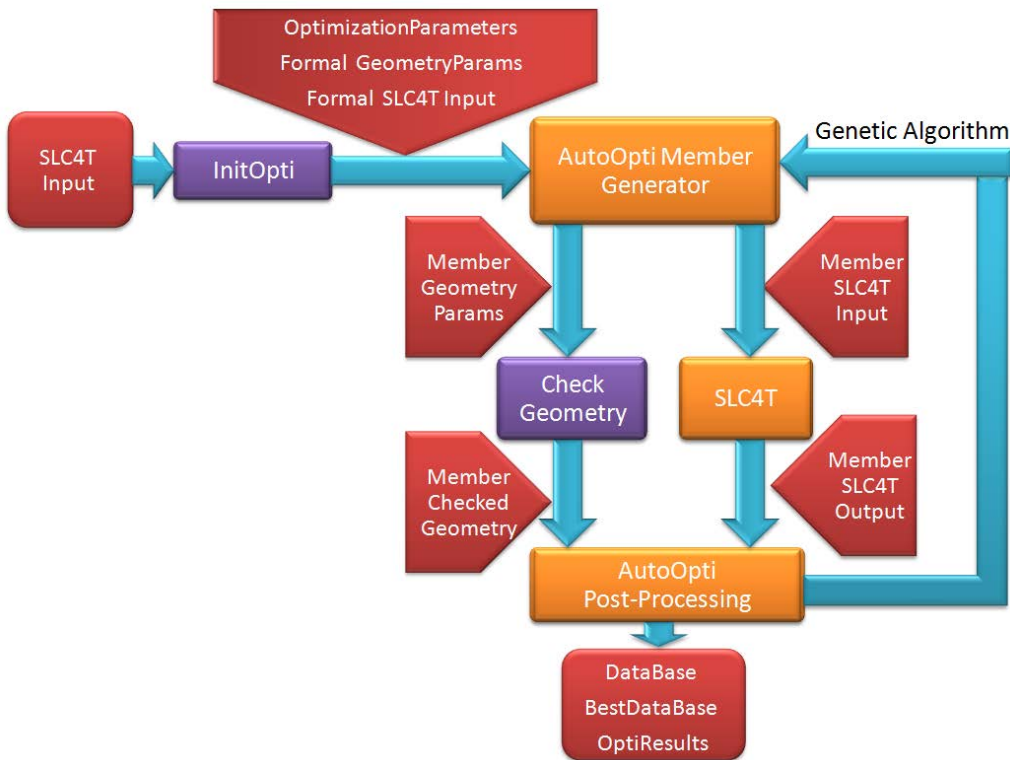


Figure 47: Process chain for annulus contour optimization - Implementation

- InitOpti*: The annulus contour geometry will be modified automatically by AutoOpti, by modifying the values of the free *OptimizationParameters*. Therefore the program *InitOpti* aims to prepare the *OptimizationParameters* and the formal input files that are going to be used for the optimization process. The *SLC4T Input* file indeed has to be slightly modified, by replacing the initial values of the *OptimizationParameters*, by the formal name of the *OptimizationParameters*.
- AutoOpti Member Generator*: AutoOpti is then in charge to replace the formal names of the *OptimizationParameters* by the values that are to be tested. The first members are generated with the help of a random function, so as to create a population of members as diverse as possible. The optimization potential may be indeed all the higher than the initial population of members is diverse. Once the initial population of members is generated, the next members are generated according to genetic algorithms. The members that best meet the fitness functions are then combined, so as to provide members that may meet the fitness functions more and more. In order to test a member, the *OptimizationParameters* values are replaced in the input files of the programs that are going to be executed in the optimization process. Thus the *SLC4T Input* file, as well as the *CheckGeometry* input file, called *GeometryParams*, are updated with the *OptimizationParameters* values of the member.
- CheckGeometry*: The program *CheckGeometry* calculates the annulus contour angles from the geometric parameters of the member. These annulus contour angles are then saved in the file *Checked Geometry*. They will be part of the *FlowParameters* and will be controlled by a region of interest.

- *SLC4T*: The program code *SLC4T* is then executed by *AutoOpti*. By this way the S2-flow computation is performed on the current member and its aero-thermodynamic properties are thus available.
- *AutoOpti Post-Processing*: The results provided by the programs *CheckGeometry* and *SLC4T* are then available. Therefore the *FlowParameters* values are known and the fitness functions values can be set. Thus, the pertinence of the member can be assessed. The member is graded and added in the *DataBase* according to his rank. As regards the best members, they are saved in the *BestDataBase*. They are going to be combined with the help of genetic algorithms, so as to generate the next member to be tested. The whole results concerning a member are available in a directory called *OptiResults*.

3.3.4 Blade geometry updating

The optimization process of the turbine annulus contour consists in testing different annulus geometries. The hub and tip positions at the blade leading edge and trailing edge are seen as relevant *OptimizationParameters*. The changes in the hub and tip positions have to be accompanied by the appropriated changes of the whole blade geometry, as it can be seen Figure 48.

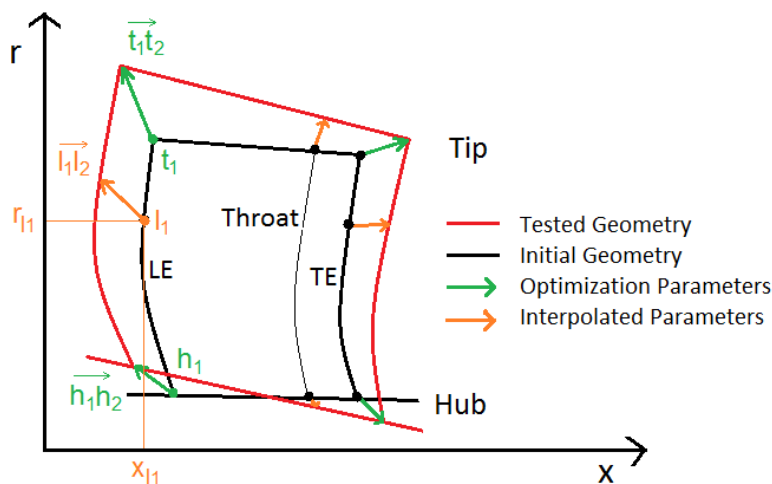


Figure 48: Blade geometry updating

Thus, the throat position and the radial distribution of the blade leading edge and trailing edge have to be interpolated. The interpolation process is detailed for the updating of the leading edge geometry. The same process has been implemented for the trailing edge, and the throat.

The initial geometric parameters are indexed with index 1, and the geometry to be tested is indexed with index 2. The change of the tip position from position 1 to position 2 can be defined by a translation vector $\overrightarrow{t_1 t_2}$. The translation of the hub position likewise is defined by a vector $\overrightarrow{h_1 h_2}$. The change of the leading edge position is parameterized by the vector $\overrightarrow{l_1 l_2}(r_{l1})$. In order to take the relative position of point (x_{l1}, r_{l1}) in relation to the hub and tip position into account, the translation $\overrightarrow{l_1 l_2}(r_{l1})$ is determined with the help of a barycentric average of vectors $\overrightarrow{t_1 t_2}$ and $\overrightarrow{h_1 h_2}$. Thus, $\overrightarrow{l_1 l_2}(r_{l1})$ is given by:

$$\overrightarrow{l_1 l_2}(r_{l1}) = \overrightarrow{h_1 h_2} * C_h(r_{l1}) + \overrightarrow{t_1 t_2} * C_t(r_{l1}) \quad (3.12)$$

The barycentric coefficients $C_h(r_{l1})$ and $C_t(r_{l1})$ are set according to the distance from point (x_{l1}, r_{l1}) to the hub position and tip position.

$$C_h(r_{l1}) = \frac{\|\overrightarrow{l_1 t_1}\|}{\|\overrightarrow{l_1 t_1}\| + \|\overrightarrow{l_1 h_1}\|} \quad \text{and} \quad C_t(r_{l1}) = \frac{\|\overrightarrow{l_1 h_1}\|}{\|\overrightarrow{l_1 t_1}\| + \|\overrightarrow{l_1 h_1}\|}. \quad (3.13) \quad (3.14)$$

$\|\overrightarrow{l_1 t_1}\|$ and $\|\overrightarrow{l_1 h_1}\|$ are the distance from l_1 to t_1 and from l_1 to h_1 respectively. By this way, the local translation of the leading edge $\overrightarrow{l_1 l_2}(r_{l1})$ can be determined. The use of this process in several radial positions r_{l1} provides a radial distribution of the leading edge coordinates. Hence the whole blade geometry can be deduced from the optimization parameters.

3.3.5 Optimization criteria

The fitness functions, as well as the flow parameters and their region of interest, have to be defined carefully so as to lead the optimization process according to pertinent criteria. The members indeed are graded according to the fitness functions and regions of interest, and the generation of new members is based on these criteria, since the highest graded members are combined by the genetic algorithms so as to generate new members. As regards the optimization of the turbine annulus contour, the turbine efficiency is obviously one of the quantities that have to be maximized. Since AutoOpti minimizes the fitness functions, the main fitness function *Loss* as been defined by: $Loss = 1 - \eta_{is}$, where η_{is} is the isentropic efficiency. Thus, the fitness function *Loss* can be seen as an aero-thermodynamic loss that has to be as close to zero as possible. So as to make sure that the turbine efficiency is always compared in the same conditions, the massflow difference between the tested member and the initial member is set as second fitness function. By this way, members of same efficiency will be all the better graded, than their inlet massflow is close to the initial member inlet massflow. Thus, the second fitness function, called massflow difference *MFD*, is defined by: $MFD = |\dot{m}_{in,member} - \dot{m}_{in,initial}|$. It ensures the consistency of the optimization process. As mentioned previously in paragraph 3.3.2, many flow parameters are limited in regions of interest. That is the case for the axial velocity, which is limited by a minimal value, so as to avoid detachments. So as to strengthen this measure against detachments, the regularity of the annulus contour is controlled by defining a region of interest on the annulus contour angles. The annulus contour angles are defined Figure 49.

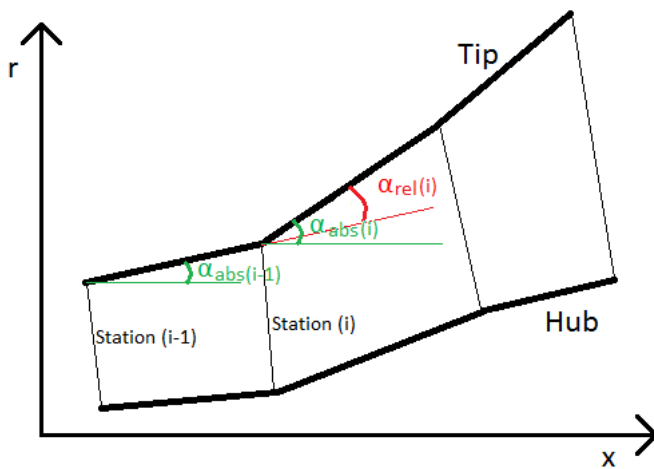


Figure 49: Definition of annulus contour angles

A pertinent quantity to ensure the annulus contour regularity is the relative angle between two consecutive stations. Hence the absolute angles $\alpha_{abs}(i)$ are calculated for each station i , and the relative angle $\alpha_{rel}(i)$ is given by $\alpha_{rel}(i) = \alpha_{abs}(i) - \alpha_{abs}(i - 1)$. The absolute angles as well as the relative angles are limited by regions of interest. Thus, the range of the optimization parameters can be even extended, while maintaining the contour regularity.

3.3.6 Test case: Hannover-Turbine

The optimization process of the annulus contour has been implemented on a 4 stages low pressure turbine, called Hannover-Turbine. The input conditions of the SLC4T computation are summed up in Table 12.

Pt_in	Tt_in	Alpha_in	Cp	R	Pt_in/Ps_out	RPM S1
[Bar]	[K]	[deg]	[J/kg/K]	[J/kg/K]	[-]	[rad/s]
2.577	404	0	1005	287.15	2.55	7500

Table 12: Hannover-Turbine - SLC4T input data

A SLC4T computation has been performed at first on the initial geometry. Some of the aero-thermodynamic properties provided by SLC4T are shown in Table 13.

Pt_in/Ps_out	Pt_in/Pt_out	m_in	m_out	Power	Specific Work	Efficiency	Tt_out
[-]	[-]	[kg/s]	[kg/s]	[kW]	[J/kg/K]	[-]	[K]
2.55	2.5052	7.42	7.42	616.4	205.61	0.8866	321.3

Table 13: Hannover-Turbine - SLC4T output data

The isentropic efficiency η_{is} provides the start value of the optimization process. The fitness function *Loss* indeed is: $Loss = 1 - \eta_{is}$. Thus the optimization process will aim to minimize the fitness function *Loss*, starting with the value: $Loss = 0.1134$. The inlet massflow $\dot{m}_{in} = 7.42$ kg/s will be considered as a reference value to be conserved by the members generated during the optimization process. The fitness function *MFD* indeed aims to minimize the massflow difference between the initial member and the current member. It is defined by: $MFD = |\dot{m}_{in,member} - \dot{m}_{in,initial}|$. A region of interest has been set on the axial velocity. Some optimization processes have been performed in order to set a pertinent limit value for this region of interest. According to these previous optimization tests, the required axial velocity limit value has been set to 17 m/s. Another region of interest has been set on the annulus contour angles, so as to preserve the contour regularity. The optimization parameters are the radial positions of non-bladed quasi-normal stations and blade leading edge and trailing edge stations. For each station, the range is set to 5% of the radius difference between the hub and the tip. The position of the throat stations is interpolated according to the method developed in paragraph 3.3.4. Two optimization computations are presented: Computation 1 has been performed without any limitation on the annulus contour angles. The region of interest on the annulus contour angles has been added for computation 2. The optimization parameters and optimization criteria of computation 1 and computation 2 are summed up Figure 50.

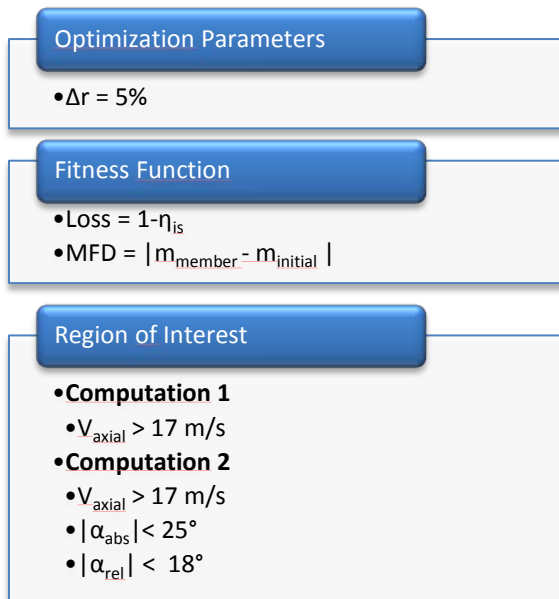


Figure 50: Optimization criteria

An overview of the members tested during the computation 1 is provided Figure 51.

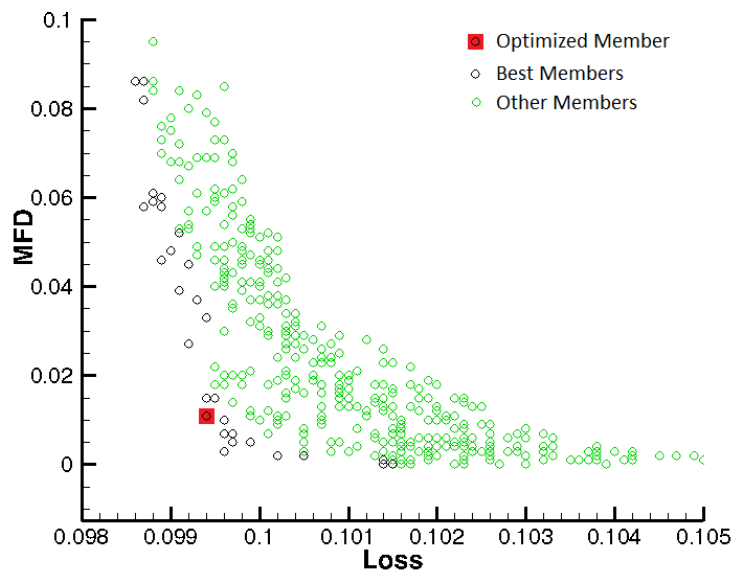


Figure 51: Hannover-Turbine - Annulus contour optimization - Computation 1

Thanks to the genetic algorithms, the generated members are rapidly better than the initial one. Therefore, the initial member is not to be seen on this map. The members are graded by taking account of both fitness functions. Therefore the distribution of some graded members is set more or less on a circle. The choice of the best member is at the discretion of the user. In most cases a compromise has to be done. The member that seems to best satisfy the fitness functions *MFD* and *Loss* is depicted in red. This member is considered as the optimized member. An overview of the initial member and the optimized member provided by computation 1 is given Figure 52.

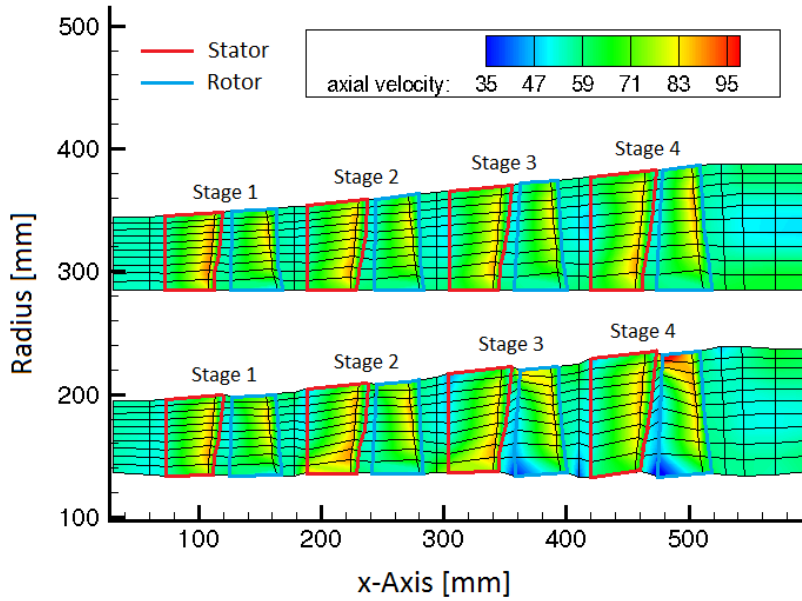


Figure 52: Hannover-Turbine - Initial Member VS Optimized Member - Computation 1

As regards the optimized member provided by computation 1, obtained without any angle limitations, a general trend can be observed: stators and rotors are slightly offset in relation to each other. This trend is especially noticeable for stage 3 and stage 4. This row configuration induces a higher axial velocity on the rotor tip, what may contribute to increase the enthalpy variation. By this way the power delivered to the spool is higher and therefore the efficiency is increased. In the rotor hub, the velocity is lower than the one in the mean line, but not inferior to 35 m/s, what is in accordance with the lowest value required by the region of interest. However it may be feared that the significant contour irregularities induce detachments, even if the axial velocity is not especially low. Therefore the region of interest has been set on the annulus contour angles for computation 2, so as to ensure a better contour regularity. The members tested during computation 2 are provided Figure 53.

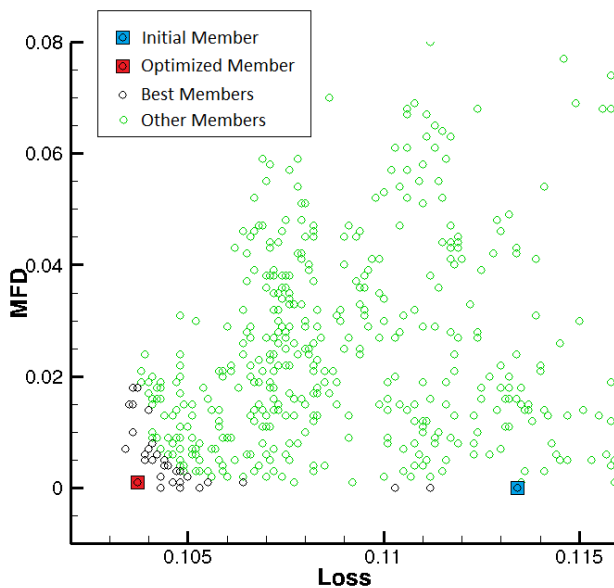


Figure 53: Hannover-Turbine - Annulus contour optimization - Computation 2

As regards computation 2, the optimization process doesn't provide so high improvements than computation 1 does. The optimized member indeed reaches only: $Loss_{comp\ 2} = 0.1037$, whereas computation 1 provided $Loss_{comp\ 1} = 0.0994$. The contour geometry indeed is more limited for computation 2, which reduces the potential of optimization. An overview of the optimized member provided by computation 2 ($\Delta r = 5\%$, $\Delta\alpha = 18^\circ$) is given Figure 54. For comparative purposes the initial member as well as the optimized member provided by computation 1 ($\Delta r = 5\%$) are given.

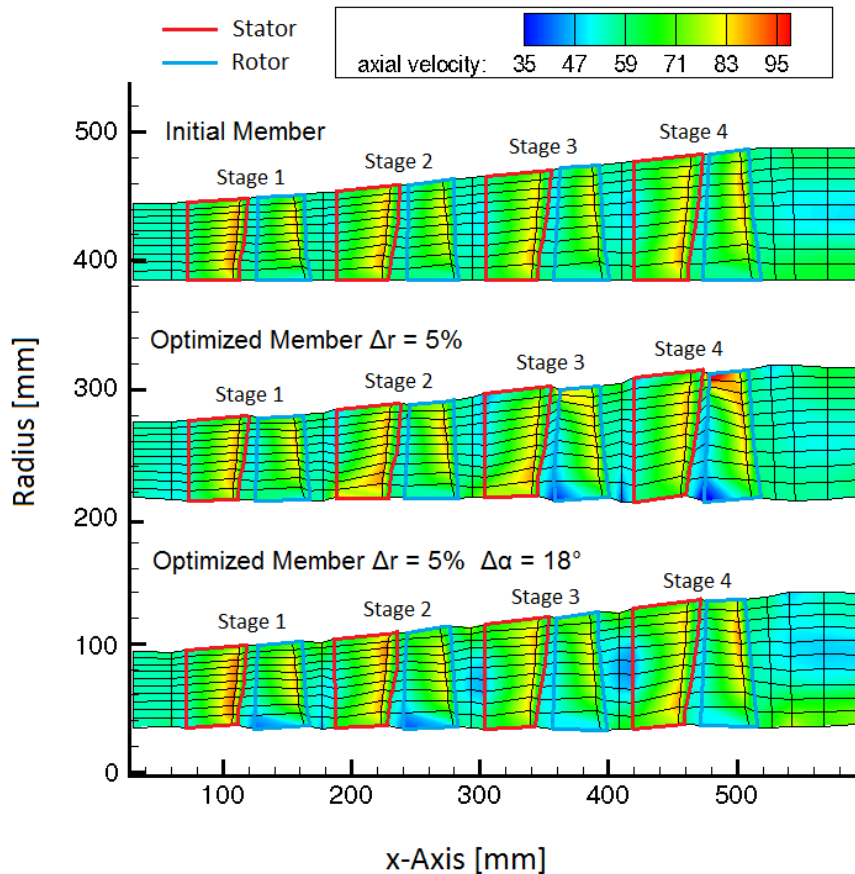


Figure 54: Hannover-Turbine - Initial Member VS Optimized Member - Computation 1, 2

The optimized member provided by computation 2, has been obtained by limiting the annulus contour angles. Therefore the annulus contour is significantly more regular, which is of great interest for aerodynamic and manufacturing considerations. The offset that could be seen between stators and rotors for computation 1 is not so noticeable as regards computation 2. However the non-bladed stations between two consecutive stages are more tighten. The annulus tip radius indeed slightly decreases, which induces flow accelerations close to the tip. Close to the hub, the flow axial velocity decreases a little, what is especially to be noticeable for stages 1 and 2. These flow velocity changes are however less worrying for computation 2 than for computation 1.

As a conclusion it would be of interest to assess the potential of optimization. The isentropic efficiencies $\eta_{iS} = 1 - Loss$, are plotted in Figure 55.

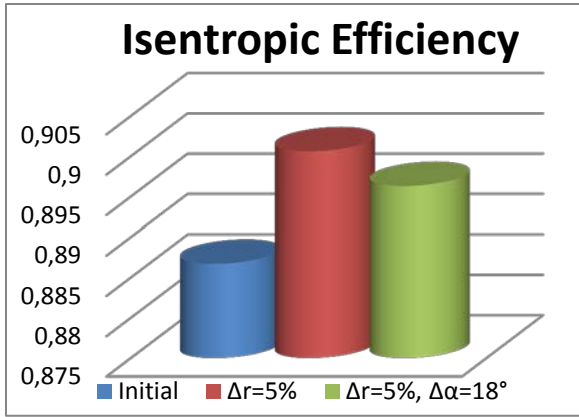


Figure 55: Hannover-Turbine - Isentropic efficiency - Optimized members - Computation 1,2

It is not to be denied that the efficiency is higher when the annulus angles are not limited at all. The potential of optimization PO_{η} has been defined as: $PO_{\eta} = \left| \frac{\eta_{is\ comp\ 1,2} - \eta_{is\ init}}{\eta_{is\ init}} \right|$. For computation 1, $PO_{\eta 1} = 1.57\%$, and for computation 2, $PO_{\eta 2} = 1.08\%$. The potential of optimization has been plotted for many flow parameters in Figure 56.

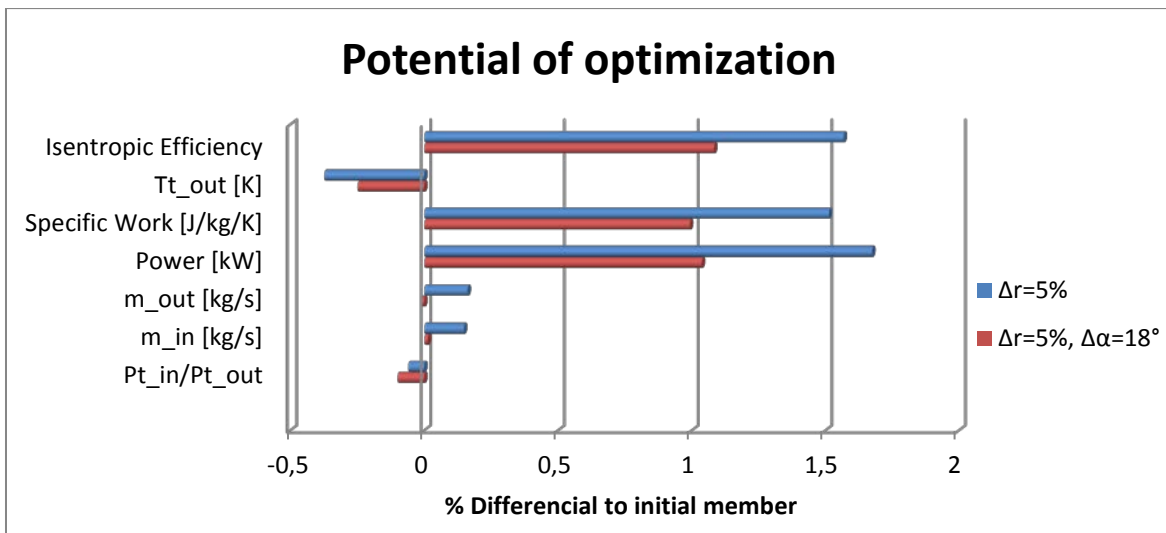


Figure 56: Hannover-Turbine - Potential of optimization - Optimized members - Computation 1,2

Since the specific power SW , defined by $SW \left[\frac{J}{kg \cdot K} \right] = \frac{Power [W]}{m_{Outlet} \left[\frac{kg}{s} \right] \cdot Tt_{in} [K]}$ and the isentropic efficiency η_{is} , defined by $\eta_{is} = \frac{Power [W]}{m_{Outlet} \left[\frac{kg}{s} \right] \cdot \Delta H_{is} \left[\frac{J}{kg} \right]}$, are proportional to the power, the same trend is to be observed for these three quantities. The massflow computed by computation 1 ($\Delta r = 5\%$), is a little higher than the one computed by computation 2 ($\Delta r = 5\%, \Delta \alpha = 18^\circ$), which increases all the more the power computed by computation 1. The higher the power, the lower is the enthalpy of the fluid in the turbine outlet. Therefore, the outlet temperature decreases, when the member is optimized. Although the potential of optimization is slightly lower as the angles are limited, the regularity of the annulus contour is seen as an important factor ensuring a better flow regularity and an easier manufacturing process. Therefore, according to aerodynamic and manufacturing considerations it may be considered, that computation 2 ($\Delta r = 5\%, \Delta \alpha = 18^\circ$) provides more satisfying results than computation 1 ($\Delta r = 5\%$).

Conclusion and prospects

The comparison between SLC4T computations and 3D-CFD computations has been of great help for the validation of the program code SLC4T. The reliability of the results indeed is soon of great advantage in the early stages of turbine design. Currently a new version of the program code SLC4T is being implemented in which the heat capacity ratio γ is iteratively calculated in each computation node. As a result, the computation time is significantly increased. The improvements as regards the precision of the results provided by this new version should be assessed. The integration of these S2-computations in the turbine pre-design process should contribute to accelerate significantly the switch from one step to the next. Some routines have been implemented, so that 1D pre-design can be followed automatically by SLC4T computations, which can provide turbine maps data files. The S2-computations are performed as well in the optimization process of annulus contours. Many optimization criteria, such as the range values of regions of interest, are strong problem-oriented. Therefore the optimization process probably has to be performed several times with trial and errors, until a satisfying optimized contour may be obtained. As regards S1-stream surfaces, human know-how is deeply involved for the design of blade profiles. The automation of blade design itself is therefore not foreseen. However, it would be of interest to implement an automatic update of S2-flow computations input files, once the blades have been designed precisely. By this way the optimization process of the annulus contour could be performed on the turbine with updated blade parameters. Furthermore as HPT and LPT are optimized together, it could be of interest to optimize the inter turbine duct shape as well. The current optimization process does not possess enough criteria, so as to provide a pertinent optimized size of the inter turbine ducts. Therefore, SLC4T computations could be complemented by boundary layer computations in the inter turbine duct.

Acknowledgements

Thank you very much to Dr. Friedrich Kost for his assistance and the lot of advice concerning the use of his program code SLC4T. Thank you to Andreas Pahs for the 3D-CFD computations.

Vielen Dank Alexander für deine Betreuung!

References

- [1] : *A General Theory of three-dimensional flow in subsonic and supersonic turbomachines of axial-, radial-, and mixed-Flow Types*, Chung-Hua Wu, Lewis Flight Propulsion Laboratory Cleveland, Ohio, 1952 ;
- [2] : *Significance of Loss Models in Aerothermodynamic Simulation for Axial Turbines*, Ning Wei, Royal Institute of Technology, Department of Energy Technology, 2000 ;
- [3] : *Improved Profile Loss and Deviation Correlations for Axial-Turbine Blade Rows*, Junqiang Zhu, Steen A. Sjolander, Carleton University, Department of Mechanical and Aerospace Engineering Ottawa, Ontario, Canada, 2005 ;
- [4] : *A method of performance estimation for axial flow turbines*, Ainley, D.G., Mathieson, G.C.R., ARC R&M 2974, 1951 ;
- [5] : *Improvements to the Ainley-Mathieson Method of turbine performance prediction*, Dunham, J., Came, P.M., Trans. ASME, J. Eng. Power, 1970 ;
- [6] : *A Mean Line Prediction Method for Axial Flow Turbine Efficiency*, Kacker, C., Okapu, U., ASME paper No. 81-GT-58, 1981 ;
- [7] : *A reduced-order through-flow program for choked and cooled axial turbines*, Carlsson, I., Lund University, 2005 ;
- [8] : *An Empirical Prediction Method for Axial Secondary Losses in Turbines – Part 1: A New Loss Breakdown Scheme and Penetration Depth Correlation*, Benner, M.W., Sjolander, S.A., Moustapha, S.H., J. of Turbomachinery, Vol 128, p.273, 2006 ;
- [9]: *A Streamline Curvature Through-Flow Computer Program for Analysing the flow through Axial-Flow Turbomachines*, D.H. Frost, National Gas Turbine Establishment, London, 1970 ;
- [10]: *Ein Verfahren zur Berechnung der Meridionalströmung von Axialturbinen*, Kost, F., DLR, 2012 ;
- [11]: *Flugzeugtriebwerke*, Bräuling, Willy J. G., HAW-Hamburg, Dep. Fahrzeugtechnik und Flugzeugbau , 2009 ;
- [12]: *Propulsion Aéronautique et Spatiale*, Gressier J., ISAE-Supaéro, 2010.

Appendix

A1 - Conservation laws for the Streamline Curvature Method

The flow properties are calculated thanks to conservation laws applied in a control surface. A control surface is defined between two consecutive stations and two consecutive streamlines. An example is given Figure 57. The conservation laws are applied in the control surface between station i and station $i + 1$.

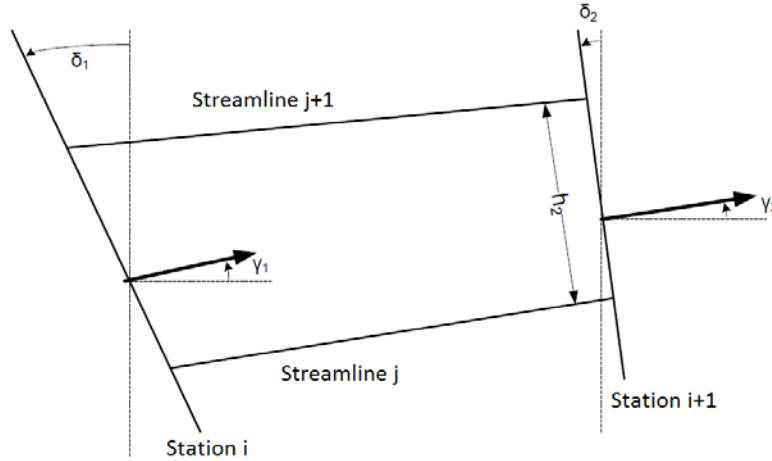


Figure 57: Control surface

- Mass conservation

$$\begin{aligned} \dot{m}_i &= \rho_i v_{x_i} \pi (r_{i,j+1}^2 - r_{i,j}^2) \\ \dot{m}_i &= \dot{m}_{i+1} \end{aligned} \quad (\text{A1.1})$$

- Impulse equation in meridional direction

$$\begin{aligned} q_i &= \dot{m}_i v_{m_i} + p_i \cdot 2\pi (f_p + r_i h_i \cos(\delta_i - \gamma_i)) \\ \text{With } f_p &= 1/6 [2r_i h_i + 2r_{i+1} h_{i+1} + r_i h_{i+1} + r_{i+1} h_i] \\ q_i &= q_{i+1} \end{aligned} \quad (\text{A1.2})$$

- Angular momentum conservation

$$\begin{aligned} L_i &= r_i v_{u_i} \\ L_i &= L_{i+1} \end{aligned} \quad (\text{A1.3})$$

- Energy conservation

$$\begin{aligned} h_{t_i} &= c_p T_{t_i} \\ h_{t_i} &= h_{t_{i+1}} \end{aligned} \quad (\text{A1.4})$$

When c_p is supposed constant, then $T_{t_i} = T_{t_{i+1}}$.

A2 – Outlet flow angle correlation

with index o to the trailing edge station with index 2. In the radial direction, this control surface is defined from the streamline j to the streamline j+1. The annular surface in the trailing edge station and in the throat station are respectively: $A_2 = \pi(r_{2,j+1}^2 - r_{2,j}^2)$, $A_o = \pi(r_{o,j+1}^2 - r_{o,j}^2) \cdot \frac{o}{t}$, as it can be seen Figure 58. For quasi parallel streamlines, we have $r_o \approx r_2$. Hence, we have : $\frac{A_o}{A_2} = \frac{o}{t}$.

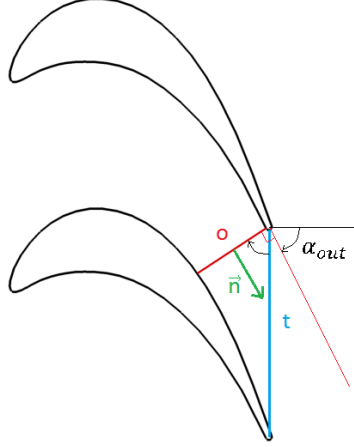


Figure 58: Cosinus Law

The massflow conservation from the throat to the trailing edge can be written with discharge of a cooling air massflow : $\dot{m}_2 = \dot{m}_o + \dot{m}_c$.

We have: $\dot{m}_2 = \rho_2 A_2 \vec{V}_{2,rel} \cdot \vec{n}$, with :

\vec{V}_2 : the trailing edge flow velocity,

ρ_2 : the fluid density,

\vec{n} : the normal vector to the throat.

That means: $\dot{m}_2 = \rho_2 A_2 W_{2,rel} \cdot \cos(\alpha_2)$, with:

$W_{2,rel}$: the relative trailing edge flow velocity in the (x, φ)-plane,

α_2 : the trailing edge flow angle.

The trailing edge massflow can be written as follows:

$$\dot{m}_2 = A_2 M_2 \frac{p_{t_{rel,2}}}{\sqrt{T_{t_{rel,2}}}} \left(1 + \frac{\gamma-1}{2} M_2^2\right)^{-\frac{\gamma+1}{2(\gamma-1)}} \cos(\alpha_2) \sqrt{\frac{\gamma}{R}} \quad (\text{A2.1})$$

- **Transonic case**

Many of modern turbines are designed so that, the Mach number $M_o = 1$ in the throat. Hence we have: $\dot{m}_o = \rho_o a_s A_o$, with:

$\rho_o = \frac{p_o}{RT_o}$: the density, calculated with the help of the static pressure and static temperature,

$a_s = \sqrt{\gamma RT_o}$: the critical sound speed.

Thus the massflow \dot{m}_o can be calculated. With a choc calculation, the flow parameters $pt_{rel,2}$, $Tt_{rel,2}$, M_2 can be calculated. Thanks to the massflow conservation $\dot{m}_2 = \dot{m}_o + \dot{m}_c$, the blade outlet flow angle α_2 can be determined.

- **Subsonic case**

When $M_o < 1$, the trailing edge flow angle is calculated with the same massflow conservation equation. The throat massflow has to be written as follows, because the sonic Mach number is not reached in the throat:

$$\dot{m}_o = A_o M_o \frac{pt_{rel,o}}{\sqrt{Tt_{rel,o}}} \left(1 + \frac{\gamma-1}{2} M_o^2\right)^{-\frac{\gamma+1}{2(\gamma-1)}} \sqrt{\frac{\gamma}{R}} \quad (A2.2)$$

The throat and the trailing edge are really close one to another. Hence, in this subsonic case, the continuity of the flow quantities is used to do the approximation $M_o \approx M_2$. Thus, thanks to the equation: $\dot{m}_2 = \dot{m}_o + \dot{m}_c$, the blade outlet flow angle α_2 can be determined :

$$\cos(\alpha_2) = \frac{A_o pt_{rel,o} \sqrt{Tt_{rel,2}}}{A_2 pt_{rel,2} \sqrt{Tt_{rel,o}}} \left(1 + \frac{\dot{m}_c}{\dot{m}_o}\right) \quad (A2.3)$$

Thanks to the rothalpy conservation we have: $Tt_{rel,2} = Tt_{rel,o}$.

Some blade loss correlations are used to calculate the ratio: $\frac{pt_{rel,o}}{pt_{rel,2}}$. By this way the outlet flow angle can be calculated in subsonic cases.